

POLITECNICO DI TORINO

Master's Degree in Nanotechnologies for ICTs



Master's Degree Thesis

Inverse Magnetolectric effect in micro and nanostructures

Supervisors

Prof. Carlo RICCIARDI

Christoph ADELMANN

Florin CIUBOTARU

Candidate

Erika GIORGIONE

2022/2023

Summary

The inverse Magnetolectric (ME) effect is a phenomenon that delineates the relationship between electricity and magnetism. Specifically, it reveals that the application of a magnetic field (H) results in a alteration in electrical polarization (P). In this thesis, the inverse ME effect is examined in multilayer composites, particularly those incorporating piezoelectric/magnetostrictive materials. Piezoelectricity denotes the ability of dielectric material to generate electrical potential under mechanical stress and vice-versa, and in some cases piezoelectric material can exhibit a ferroelectric behavior. Ferroelectricity is a physical property that describes the presence of a spontaneous electrical polarization that can be switched by the application of an electric field. On the other hand, magnetostriction, is a distinct property of ferromagnetic materials to expand or contract when subjected to a magnetic field, effectively converts electromagnetic energy into mechanical energy. The investigated stack involves PVDF-TrFe as piezoelectric layer and Ni as magnetostrictive layer. In this composite, when an external magnetic field is applied, the interaction between the two layers facilitates the transfer of deformation induced by magnetostriction to the piezoelectric component, resulting in dielectric polarization. The devices fabrication process involves spinning a 500 nm thick PVDF-TrFe on either $Si - SiO_2(400nm)/Ta(10nm)/Pt(100nm)$ substrate or directly on a Ni foil substrate. Subsequently, the PVDF-TrFe layer is baked before at 70 °C in vacuum and then at 140 ° in N_2 atmosphere. After that, Nickel and Gold dots are either evaporated or sputtered onto the PVDF-TrFe substrate on top of $Si - SiO_2/Ta/Pt$, while only Gold dots are evaporated on top the PVDF-TrFe substrate on Ni foil. The dots come in varying diameters according to the pattern provided by a shadowed mask. Polarization of the PVDF-TrFe consists in 80 V peak to peak triangular waves at 50 Hz for 200 pulses, which allows the PVDF-TrFe structure to transition from the α -phase to β -phase, characterized by the highest dipolar moment. The ferroelectric and piezoelectric behavior of PVDF-TrFe has been demonstrated by measuring its Polarization-Voltage (P-V) loop. However, in sputtered samples, the loop results to be very leaky, due to atom implantation in the PVDF-TrFe itself. On the other hand, P-V loops evaporated sample show a clear ferroelectric behavior. Moreover, measurements of Capacitance (C-V loop) are

conducted using an LCR meter, revealing the classical butterfly loop of ferroelectric materials. Subsequent measurements involve the simultaneous application of a magnetic field In Plane (IP) and Out Of Plane (OOP). The OOP magnetic field varies from -1 Tesla to 0 and from 1 Tesla to 0, while the IP field remains fixed at 500 Oe (0.05 T). This configuration allows to fully saturate the Ni layer IP and gradually rotate the magnetization OOP while increasing the OOP external field. The PVDF layer was subjected to the same poling conditions as mentioned earlier, and its P-V loop was measured in relation to the OOP magnetic field. The results indicated that materials experienced a degradation during the measurements. To mitigate this degradation issue, the solution adopted was the reduction of the number of the pulses in the poling step to 10 during the measurement. In this way, the degradation is reduced from 40 % to 2.5 %. What comes next is the evaluation of the polarization dependence on the magnetic field. However, measurement noise exceeded the expected polarization variations estimated by the material properties. This noise may be attributed to inadequate setup isolation and suboptimal device mounting. An alternative approach to estimate the inverse ME coupling could involve measuring the charges generated by the ME effect rather than focusing solely on polarization.

Acknowledgements

First of all, I would like to express my sincere gratitude to Imec. In this extraordinary environment, I had the opportunity to immerse myself for the first time in the world of work and research, and I was completely fascinated by it. I am grateful for meeting people from all over the world, ready to share their experiences and offer help in every challenging moment.

I would like to extend deep thanks to my supervisors, Christoph Adelman and Florin Ciubotaru, for the work done together in these months. Their constant guidance, resolution of doubts, and valuable advice have significantly contributed to the success of this project.

Special thanks go to Federica Luciano, who accompanied me daily on this thesis journey. I will never stop thanking her for the valuable help and the things she has taught me. It is thanks to her that I became passionate about the work carried out in these months. Also, thanks for the psychological support and the shared beers; we will see each other soon in our region.

I want to thank Prof. Carlo Ricciardi as my Master's thesis supervisor at Politecnico di Torino.

An immense thank you goes to my parents. Thank you for always believing in me, for understanding my difficulties, for the comforting words you dedicate to me every evening on the phone. I deeply appreciate your love, your admiration, and I hope never to disappoint you in life.

A special thanks to my sisters, to Lorianana because despite being a bit different, she always manages to convey her affection to me through small gestures and many cakes, to Roberta, simply for always being there for each other, and for being my other half.

A special thanks goes to the one who is like a brother to me, to Raffaele. In these last few years, we have built a very deep bond. Thank you for the trust you have given me, and, above all, thank you for being there for me in every moment, always trying to make me laugh with your humor.

My deepest thoughts at this moment in my life go to my grandparents. I am very

sorry that I cannot share this goal with you, but I hope I have made you proud. I miss you unconditionally.

The biggest thanks goes to the person who has changed my life, Chicca. Thank you for always making me happy and carefree, because every single photo, word, or gesture from you brings a smile to my face.

Thanks to the rest of my family for the welcome you give me every time I come home.

Thanks to my lifelong friends because no matter where I am in the world, you are always there for me.

An immense thank you to Turin, the city that stole my heart and allowed me to meet wonderful people who helped me grow and change for the better. Thanks to my Turin family for the trips and the countless days and evenings spent together. We faced this journey always together, and my achievement is also yours because without your great support and the countless study sessions filled with both hard work and laughter, I would never have made it. Each of you has taught me something, and I will never stop thanking you for all the goodness you show me every time.

An infinite thank you to all my Belgian friends; it has been a phenomenal experience. Thank you for the evenings, dinners, festivals, and trips we shared together. I will always carry you in my heart.

Table of Contents

List of Tables	IX
List of Figures	X
Acronyms	XIV
1 Introduction	1
1.1 Introduction on the Inverse Magnetoelectric effect	1
1.2 Magnetostrictive/piezoelectric composites	3
1.2.1 Piezoelectric and ferroelectric materials	3
1.2.2 Magnetostrictive material	9
1.3 Single-phase ME materials: multiferroics	12
1.4 Conclusion	14
2 Fabrication process and material characterization	16
2.1 Nickel	16
2.1.1 Vibrating-sample magnetometry (VSM) analysis	18
2.2 Nickel foil	19
2.3 PVDF-TrFe	21
2.3.1 Polarization-Voltage loops	23
2.3.2 LCR meter measurements	25
3 Inverse ME effect measurements	31
3.0.1 Description of the setup and measurement technique	31
3.1 Inverse ME effect measurements for the device: $Si - SiO_2/Ta/Pt -$ PVDF-TrFe- Ni and Au dots	33
3.2 Inverse ME effect measurements for the device: PVDF-TrFe on Ni foil	38
3.3 Outlook	40
3.3.1 Charge measurements	40
4 Conclusions	42

List of Tables

2.1	Value of Hysteresis loop	20
2.2	Values of P-V loop	25

List of Figures

1.1	Schematic representation of the device used to demonstrate the Magnetoelectric effect in Antiferromagnet. ⁽⁷⁾	2
1.2	Polarization vs. electric field (P-E) hysteresis loop in ferroelectric materials. ⁽⁸⁾	4
1.3	Schematic representations showing the alignment of ferroelectric domain and macroscopic strains when a ferroelectric material is subjected to a poling treatment under electric field . (a) Initial state (b) Saturation State (b) Remanent state. ⁽⁸⁾	5
1.4	Polymer structure of β phase in PVDF crystals. ⁽⁵⁾	7
1.5	XRD patterns of the starting PVDF powder and PVDF flms cast from solvents of THF, MEK, DMF, and DMSO at 50 °C crystallization temperature. ⁽⁹⁾	8
1.6	FTIR patterns for PVDF flms treated with THF, MEK, DMF, and DMSO and crystallized at 50 °C. ⁽⁶⁾	9
1.7	Schematic pictures that show how Magnetostriction varies quadratically with strain and piezomagnetism varies linearly. ⁽¹³⁾	10
1.8	Typical magnetostriction curves in form of butterfly loop. ⁽¹¹⁾	10
1.9	Schematic drawing depicting the magnetostriction caused by rotation of magnetization. ⁽¹¹⁾	11
1.10	Magnetostriction curves characteristic of Ni (thick) and Fe(thin). ⁽¹¹⁾	12
2.1	Schematic representation showing the standard sputtering technique. ⁽¹⁶⁾	17
2.2	Schematic representation showing the thermal evaporation technique. ⁽¹⁷⁾	17
2.3	Schematic picture of (a) part of the VSM setup and (b) types of holder used in VSM. ⁽¹⁸⁾	18
2.4	Hysteresis loop OUT OF PLANE Magnetization-Applied field for four different samples.	19
2.5	Hysteresis loop OUT OF PLANE Magnetization-Applied field (a) and IN PLANE Magnetization-Applied field (b) for Ni foil.	20

2.6	Schematic image of the two stacks: PVDF on Si/SiO_2 and Pt (a), PVDF on Ni foil (b).	21
2.7	Schematic representation of the preparation of β -PVDF by spin coating. With the help of a syringe the PVDF solution is deposited on the substrate located on the rotary disk of the spin coater; proceed the deposition step at rotational velocity of 4000 rpm for 30 s; place the film onto a hot plate at 70 °C; and the PVDF film is ready. ⁽¹⁹⁾	22
2.8	Schematic pictures of the final device: $Si/SiO_2/Ta/Pt/PVDF-TrFe$ and on top dots of Ni and Au evaporated (a), $Si/SiO_2/Ta/Pt/PVDF-TrFe$ and on top dots of Ni and Au sputtered (b), Ni foil+PVDF-TrFe on top dots of Au evaporated (c).	23
2.9	Polarization-Voltage (P-V) loop of the three different devices: Ni/Au evaporated (a), Ni/Au sputtered (b), Au evaporated (for PVDF-TrFe on Ni foil) (c).	24
2.10	CV loops- Frequency 1 kHz(a,b), Frequency 10 kHz (c,d), Frequency 100 kHz (e,f), Frequency 1 MHz (g,h) for different structures: 60 μm , 90 μm , 120 μm , 150 μm [left] 200 μm , 300 μm , 400 μm and 500 μm [right].	27
2.11	CV loops of the structure 200 μm at different frequencies: 1 kHz, 10 kHz, 100 kHz, 1 MHz.	28
2.12	Dielectric constant (ϵ_R)- Frequency 1 kHz(a), Frequency 10 kHz(b), Frequency 100 kHz(c), Frequency 1 MHz (d) for different structures: 60 μm , 90 μm , 120 μm , 150 μm , 200 μm , 300 μm , 400 μm and 500 μm	29
2.13	CV loops for device : Ni foil/PVDF-TrFe/Au evaporated- Frequency 10 kHz (a), Dielectric constant (ϵ_R)- Frequency 10 kHz (b) for different structures: 60 μm , 90 μm , 120 μm , 150 μm , 200 μm , 300 μm , 400 μm and 500 μm	30
3.1	Picture of the setup used for inverse ME measurements (a), zoom on the magnets (b).	32
3.2	PV loops of the structure 300 μm applying: (a) OOP magnetic field from -1 Tesla to 0 and from 1 Tesla to 0 (b) IP magnetic field constant 500 Oe (0.05 T) and OOP magnetic field from -1 Tesla to 0 and from 1 Tesla to 0.	34
3.3	Representation of how remanence polarization varies applying a OOP magnetic field (from -1 Tesla to 0 and from 1 Tesla to 0) for a structure of 300 μm : negative remanence (a) and positive remanence(b), Representation of how remanence polarization varies with the number of measurements for a structure of 300 μm : negative remanence (c) and positive remanence(d).	35

3.4	Representation of how coercive field and saturation varies with the application of magnetic field with the number of measurements for a structure of 300 μm : negative coercivity (a) and positive coercivity (b), negative saturation (c), positive saturation (d).	36
3.5	100 Polarization-Voltage (P-V) loops for a structure of 400 μm :(a) Initial Poling (200 pulses) + successive measurements (10 pulses);(b) Initial poling (200 pulses) + successive measurements (200 pulses). .	37
3.6	Representation of how normalized Remanence Polarization for a structure of 400 μm varies: (a) Comparison of 100 measurements conducted with 200 pulses or 10 pulses; (b) Zoom on the measurements with 10 pulses	37
3.7	Polarization-Voltage (P-V) loop for a structure of 400 μm for a device fabricated with PVDF layer on top of Ni foil: OOP field (a), IP field constant OOP field variable (b).	38
3.8	Representation of how positive and negative remanence polarization varies with the application of magnetic field OOP [-1 Tesla to 0 and 1 Tesla to 0](a,b) and IP CONSTANT [500 Oe]- OOP [-1 Tesla to 0 and 1 Tesla to 0] (c,d) for a structure of 400. μm	39
3.9	Representation of charge induced by ME effect for a structure of 200 μm and 500 μm	41

Acronyms

ME: MagnetoElectric
H: Magnetic field
P: Polarization
V: Voltage
E: Electric field
M: Magnetization
P-V: Polarization-Voltage
 ϵ_R : Dielectric constant
Y: Young Modulus
Q: Charges
C-V: Capacitance-Voltage
 Cr_2O_3 : Chromium(III) oxide
PVDF-TrFe: Poly (vinylidene fluoride-trifluorethylene)
Si: Silicon
 SiO_2 : Silicon Oxide
Ta: Tantalum
Pt: Platinum
 $BiFeO_3$: Bismuth ferrite
 Fe_3O_4 : Iron(II,III) oxide
 $YMnO_3$: Hexagonal manganite
 d_{33} : Piezoelectric charge coefficient
 g_{33} : Piezoelectric voltage coefficient
k: Electro-mechanical coupling coefficient
 k^T : Relative dielectric constant at a constant stress
 s^E : Elastic compliance at constant electric field
x: Piezoelectric Coupling Coefficient
DMSO: Dimethyl sulfoxide
DMF: Dimethylformamide
MEK: Methyl ethyl ketone
THF: Tetrahydrofuran
XRD: X-Ray diffraction

FTIR: Fourier-transform infrared spectroscopy

DC: Direct Current

RF: Radio Frequency

VSM: Vibrating-sample magnetometry

IP: In Plane

OOP: Out Of Plane

AC: Alternating Current

Chapter 1

Introduction

1.1 Introduction on the Inverse Magnetoelectric effect

The magnetoelectric (ME) effect is a phenomenon that describe the link between magnetism and electricity and it is possible to distinguish two distinct manifestations:

- **Direct Magnetoelectric Effect:** The application of an electric field (E) or voltage signal (V) causes a change in magnetization (M).
- **Inverse Magnetoelectric Effect:** The application of magnetic field (H) induces a change in electric polarization (P).

The first knowledge of ME effect dates back to 1894 with P.Curie who demonstrated the possibility to polarize an asymmetric molecular body under the influence of a magnetic field.⁽¹⁾

Then, L.D.Landau and E.Lifshitz stated that it is possible to see a linear ME effect in magnetically ordered crystals.⁽²⁾

I.Dzyakishinskii, on the basis of theoretical analysis, predicted the existence of the ME effect in single phase materials, like antiferromagnetic Cr_2O_3 .⁽³⁾ He examined the behavior of the thermodynamic potential of Cr_2O_3 under various symmetry transformation, revealing two expressions in the thermodynamic potential.

These expressions are linear in both electric field (E) and magnetic field (H), indicating a linear relationship between induction and field intensities:

$$P_i = \alpha_{ij} H_j^{(4,5)} \quad (1.1)$$

$$M_i = \alpha_{ij} E_j^{(4,5)}. \quad (1.2)$$

The proportionality coefficient α_{ij} is finite number determined by the phenomenological symmetry requirement.⁽⁶⁾

In figure 1.1 there is a schematic drawing of the device used to evaluate the magnetic moment that appears in a sample of Cr_2O_3 (1) when it is placed in an alternating electric field generated by the electrodes (2).

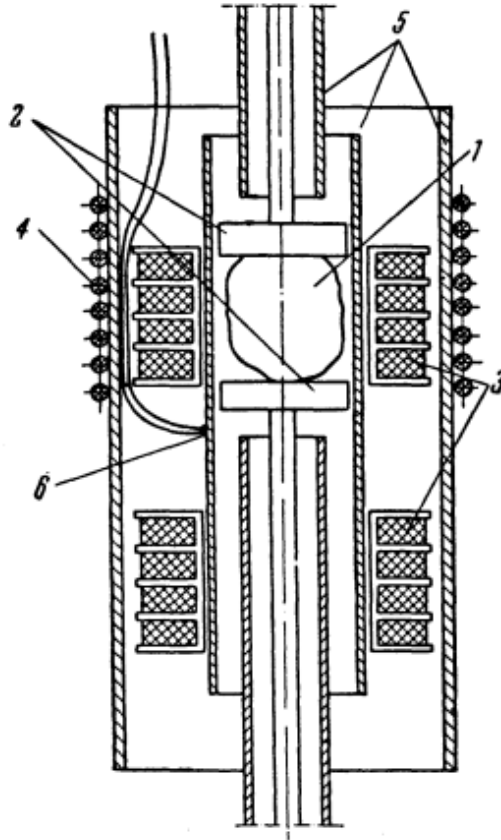


Figure 1.1: Schematic representation of the device used to demonstrate the Magnetoelectric effect in Antiferromagnet.⁽⁷⁾

Single-phase ME materials, however, often display weak ME coupling at room temperature. On the other hand, it is feasible to quantify a significantly stronger interaction in multilayer composite structures made of piezoelectric/piezomagnetic or piezoelectric/magnetostrictive multilayers.

1.2 Magnetostrictive/piezoelectric composites

In composite materials consisting of magnetostrictive and piezoelectric, the mechanical deformation brought on by the magnetostriction is transferred to the piezoelectric material, resulting in dielectric polarization. As a result, the ME effect emerges as a product property of magnetostriction effect (magneto-mechanical effect) in the ferromagnetic material and piezoelectric effect (mechanical-electrical effect) in the piezoelectric material.

$$\text{Magnetolectric effect} = \frac{\text{magnetic}}{\text{mechanical}} \times \frac{\text{mechanical}}{\text{electrical}} \quad (1.3)$$

or

$$\text{Magnetolectric effect} = \frac{\text{electrical}}{\text{mechanical}} \times \frac{\text{mechanical}}{\text{magnetic}} \quad (1.4)$$

1.2.1 Piezoelectric and ferroelectric materials

Piezoelectricity refers to a dielectric material's ability to generate an electrical potential when subjected to mechanical stress. It is possible to distinguish two different manifestations:

- **Direct Piezoelectric effect:** When a material is deformed by a mechanical stress, electrical charges are generated on its surface
- **Converse Piezoelectric effect:** When a material is subjected to an electric field, a mechanical strain is generated.

In some cases piezoelectric materials can exhibit a ferroelectric behaviour. Ferroelectricity is a physical property that describe the presence of a spontaneous electric polarization that can be switched by the application of an electric field. Furthermore, all ferroelectric materials are pyroelectrics, and all pyroelectric are piezoelectric. Pyroelectricity is the ability of a material to change its polarization state and, as a result, its generated voltage when subjected to temperature changes. Nevertheless, not all piezoelectric materials are pyroelectric, and not all pyroelectric materials are ferroelectric. As a matter of fact, ferroelectric materials are characterized by the formation of electric dipoles, whose orientation can be reversed by applying a sufficiently large electric field. On the other hand, in both piezoelectric and pyroelectric materials the formation and orientation of electric dipoles is not required.

In ferroelectric materials the polarization is not only dependent by the electric field, but also by the material's history, as demonstrated by the hysteresis P-E (polarization-electric field) loop. The P-E loop is an important criterion to distinguish if the material is ferroelectric or not, since in ferroelectric materials the

polarization shows an hysteretic behaviour due to the reaction of electric domains to an electric field. This hysteretic behavior reminds the M-H loop in ferromagnetic material, where the magnetization shows the same hysteresis as a result of the response of the magnetic domain to a magnetic field. In the figure 1.2 there is a clear representation of the typical hysteresis loop of ferroelectric materials: from the point A the polarization initially increases slowly with E-field, but turns to a sharp increases when the field reaches a certain threshold. Following then, there is a prolonged phase where the polarization steadily rises until it reaches a saturation level in point B, denoted as P_s . Successively when the E-field is removed the polarization does not return to its initial point, but it is set to a non-zero values defined as remanent polarization, P_r . To reset the polarization to zero, an E-field applied in the opposite direction is necessary. This opposing E-field is referred as coercive field, E_c , and it represents the electric field required to reverse the direction of ferroelectric polarization.

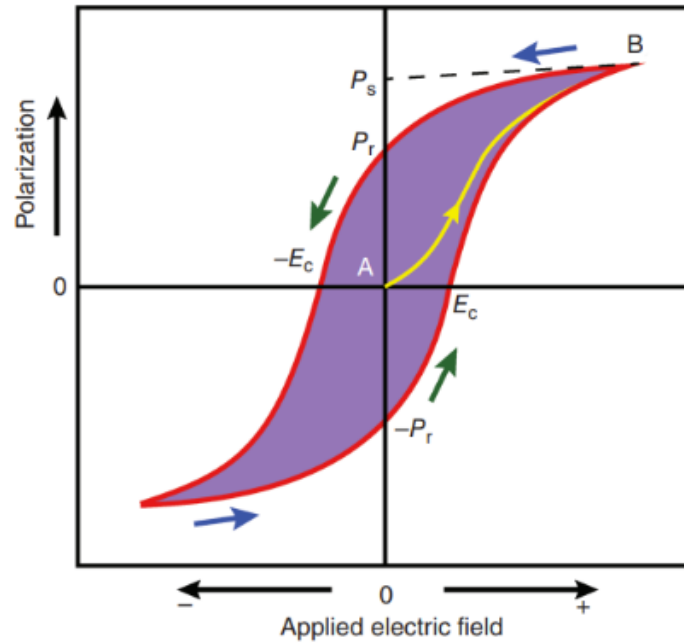


Figure 1.2: Polarization vs. electric field (P-E) hysteresis loop in ferroelectric materials. ⁽⁸⁾

The ferroelectric phase transition depends on a structural phase transition marked by ion displacements that cause changes in crystal lattice and symmetry. The extent of ion displacements in materials is determined by the crystal's specific

structure and composition. A depolarizing electric field is generated when polarization distributes equally throughout the crystal. To minimize the electrostatic energy linked to this field, the crystal tends to divide into regions known as domains. Each domain is a region with uniform polarization, and the boundaries between adjacent domains are called domain walls. The domain represents a region within a ferroelectric material where polarization is consistently aligned. The Saturation Polarization, P_s , corresponds to the total polarization when all the domains are aligned along the direction of the applied field. If the electric field is removed, part of the domain's alignment is preserved, resulting in a remanent polarization P_r . A ferroelectric material with remanent polarization can serve as a piezoelectric material, generating electric charges when subjected to mechanical stress. Essentially, polycrystalline bulk ferroelectric materials exhibit no piezoelectric response if they haven't been subjected to an electric field. This is because charges collectively cancel out when domains are randomly orientated in different directions, resulting in no change when the entire material experiences mechanical deformation. In this way, piezoelectricity is one of the functionalities of ferroelectric materials, and typically, ferroelectric materials require poling to demonstrate this feature. During the poling process, a strong electric field is applied to ferroelectric materials, causing most domains to realign along the field's direction. Figure 1.3 illustrates this poling process. To provide virtually uniform reorientation of the domains along the same direction, the applied electric field must greatly exceed the coercive field (E_C), as shown in Figure 1.3.b. This poling process causes the poled material to expand and generate tensile strains, which aligns with the converse piezoelectric effect. After poling, as shown in Figure 1.3.c, some domains may revert back to their original orientations or alter to relieve mechanical strains caused by the removal of the poling electric field. The material, after the poling treatment, exhibits a macroscopic polarization equivalent to the remanent polarization (P_r).

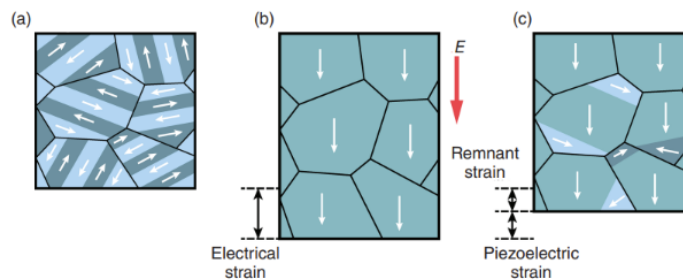


Figure 1.3: Schematic representations showing the alignment of ferroelectric domain and macroscopic strains when a ferroelectric material is subjected to a poling treatment under electric field . (a) Initial state (b) Saturation State (b) Remanent state. ⁽⁸⁾

As a result, the poling process plays a crucial role in the development of piezoelectric materials. For the same materials, incomplete poling results in drastically lower piezoelectric properties, particularly the piezoelectric charge coefficient (d_{33}). The poling procedure is not applicable to non-ferroelectric materials, underlining the necessity of ferroelectricity as a precondition for high-performance piezoelectric materials. The intensity of piezoelectric response can be estimated by using the following parameters:

- **Piezoelectric Charge (Strain) Constant (D-constant):** This is a constant that relates the electric charge generated per unit area with an applied mechanical force. It is measured in Coulomb/Newton (C/N) units.

$$d = \frac{\text{Strain developed}}{\text{Applied Field}} = \frac{\text{Charge density}}{\text{Applied stress}} \quad (1.5)$$

It is possible to relate this d constant with the materials properties through the following equation

$$d = k\sqrt{\epsilon_0 k^T s^E} \quad (1.6)$$

where k is the electro-mechanical coupling coefficient, k^T is the relative dielectric constant at a constant stress, and s^E is elastic compliance at constant electric field

The greater is the mechanical displacement, the greater is d constants. There are two d constants that can be distinguished:

$$\begin{aligned} - d_{31} &= k_{31}\sqrt{\epsilon_0 k_3^T s_{11}^E} \\ - d_{33} &= k_{33}\sqrt{\epsilon_0 k_3^T s_{33}^E} \end{aligned}$$

d_{33} represents the coefficient when the force is applied along all three directions (parallel to the polarization axis), and the charge are gathered on the surface from which the force is impressed.

Instead, d_{31} represents coefficient when the force is applied perpendicular to the polarization axis and the charges collected in the same surface of d_{33} .

- **Piezoelectric Voltage Coefficient (G-constant):** This coefficient is defined in units *voltage · meter/Newton* (Vm/N) and represents the electric field generated when the mechanical stress is applied

$$g = \frac{\text{Strain developed}}{\text{Applied charge density}} = \frac{\text{Field developed}}{\text{Applied mechanical stress}} \quad (1.7)$$

The expression for g-constant is derived from the piezoelectric charge (strain) constant(d) and the relative permittivity (ϵ)

$$g = \frac{d}{\epsilon} \quad (1.8)$$

Also in this case it is possible to categorize the g constant as g_{33} and g_{31} corresponding to d_{33} and d_{31} respectively, and also they depend on the relative directions.

- **Piezoelectric Coupling Coefficient:** this coefficient represents the mechanical energy accumulated in response to electrical energy applied.

$$x = \sqrt{\frac{\text{Mechanical energy stored}}{\text{Electrical energy applied}}} = \sqrt{\frac{\text{Electrical energy applied}}{\text{Mechanical energy applied}}} \quad (1.9)$$

Among the possible piezoelectrics in the recent years the organic materials have started to be considered promising for many new applications due to their light weight, low costs manufacturing, mechanical flexibility and the compatibility with biological systems. In particular, PVDF (polyvnylidene fluoride) and its copolymer PVDF-TrFe trifluoroethylene (TrFe) exhibit excellent electroactive properties, such as piezoelectricity, pyroelectricity and ferroelectricity. These polymers are characterized by 5 known phases: $\alpha, \beta, \gamma, \delta$ and ϵ , but the β phase exhibits the highest dipolar moment and the highest piezoelectric response. This β phase can be obtained by mechanical stretching of α phase, or through the polarization under high electric fields, or with the addition of fillers and specific nanostructures to the polymer matrix.

As it is shown in the figure 1.4, the β phase creates dipoles that are perpendicular to the chain direction and causes spontaneous polarization.

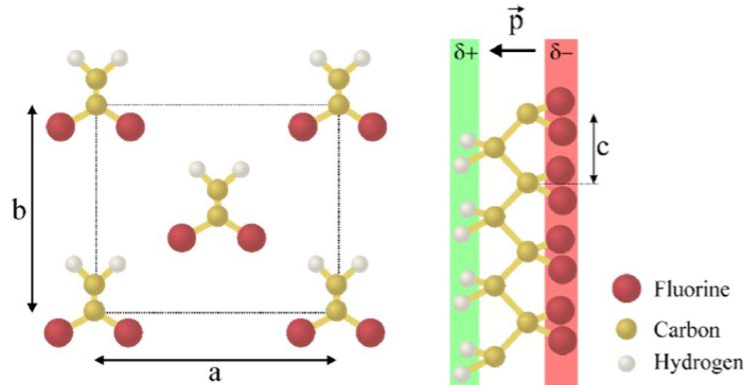


Figure 1.4: Polymer structure of β phase in PVDF crystals.⁽⁵⁾

The fabrication technique can influence the PVDF phase, in particular the addition of TrFe in the copolymer can crystallize polymer into the polar phase after thermal annealing. PVDF can be mixed with specific solvents: DMSO, DMF, MEK or THF. The crystal structure of PVDF or PVDF-TrFe films have been analyzed in literature by X-ray diffractometer and Fourier Transform infrared spectra (FTIR) from 400 to 1600 cm^{-1} .⁽⁹⁾

The crystalline fraction was determined using differential scanning calorimetry (DSC) that operate at 10 $^{\circ}C\ min^{-1}$ with an heating rate from 30 $^{\circ}C$ to 200 $^{\circ}C$.⁽⁹⁾ In the figure 1.5 is shown the XRD pattern of the PVDF films crystallized at 50 $^{\circ}C$ by using DMSO, DMF, MEK and THF as solvents. The starting PVDF powder is mainly in α phase and with six diffraction peaks at 18.2 $^{\circ}$, 19.8 $^{\circ}$, 26.4 $^{\circ}$, 32.9 $^{\circ}$, 35.8 $^{\circ}$ and 38.6 $^{\circ}$, corresponding to the crystal orientations (100), (110), (021), (031), (200) and (002). The diffraction peaks for the synthesized PVDF produced using THF solvent match those of PVDF powder α phase. On the other hand, PVDF films treated with MEK, DMF and DMSO are characterized by the β phase diffraction peak around 2θ of 20.4 $^{\circ}$, whereas α -phase diffraction peaks are smaller. It is possible to see that β phase dominates the DMSO solvent and corresponds to (110) $_{\beta}$ peak. The transformation from the original α -phase conformation (TG'TG', trans gauche) to β -phase conformation (TTTT- trans planar zigzag) in PVDF film is also showed in figure 1.5.

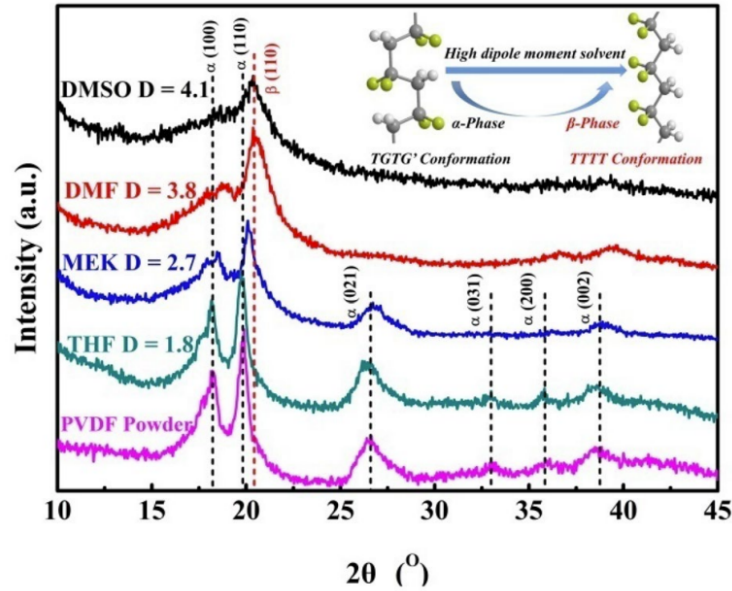


Figure 1.5: XRD patterns of the starting PVDF powder and PVDF films cast from solvents of THF, MEK, DMF, and DMSO at 50 $^{\circ}C$ crystallization temperature.⁽⁹⁾

For what regard the analysis of data with FTIR of PVDF treated with THF, MEK, DMF and DMSO, in figure 1.7 it is possible to see that for wavenumbers at 533 cm^{-1} , 617 cm^{-1} , 763 cm^{-1} and 976 cm^{-1} can be described with the α phase characteristic absorption peaks. On the other hand, the spectra 432 cm^{-1} , 510 cm^{-1} and 831 cm^{-1} are associated with the β phase characteristic absorption peaks.

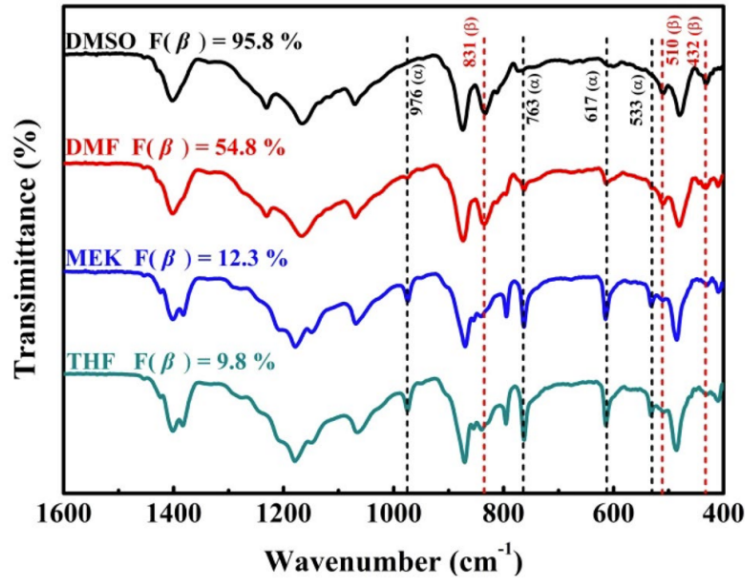


Figure 1.6: FTIR patterns for PVDF films treated with THF, MEK, DMF, and DMSO and crystallized at $50\text{ }^{\circ}\text{C}$. ⁽⁶⁾

It is possible to notice, as previously documented by the XRD diffractions, that the absorption peaks of β phase become more visible as the spectra dipole moment increases, while the absorption peaks of α phase slowly disappear. The processing technique used to achieve a specific structure can be different (e.g., doctor blade, spin coating, printing technique, ink jet printing) but the most indicated, according to the desired characteristics and applications, can be chosen. Spin coating appears to be the most suitable technology for processing film with thickness ranging from few nanometers to tens of micrometers, with great structural uniformity and reproducibility.

1.2.2 Magnetostrictive material

Magnetostriction, a distinctive property of ferromagnetic materials to expand or contract when subjected to a magnetic field, effectively converts electromagnetic energy into mechanical energy. Piezomagnetism is a phenomenon observed mostly

in antiferromagnetic crystal. While magnetostriction varies quadratically with the strain and so requires additional external magnetic fields for the magnetization reversal, piezomagnetism offers a linear coupling between the system's magnetization and mechanical strain. This unique property allows for sensitive control of magnetization using only small strains and even reverse its direction by 180° . The majority of the ferromagnetic materials exhibit the magnetostrictive effect, however the piezomagnetic effect cannot be observed in these materials.

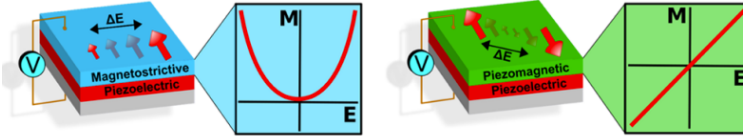


Figure 1.7: Schematic pictures that show how Magnetostriction varies quadratically with strain and piezomagnetism varies linearly. ⁽¹³⁾

In detail, it is possible to distinguish the magnetostriction effect for a ferromagnetic material in two possible outcomes:

- **Joule effect:** a ferromagnetic material can lengthen or contract when exposed to a magnetic field ;
- **Villari effect:** the reversal of previous one, the magnetization changes subjected to a mechanical stress.

Magnetostriction curves in the figure 1.8 depict the relationship between the relative deformation $\lambda = \frac{dL}{L}$, where L is the length of the sample, versus the applied magnetic field. A symmetrical shape distinguishes the hysteresis loop, known as a "butterfly loop."

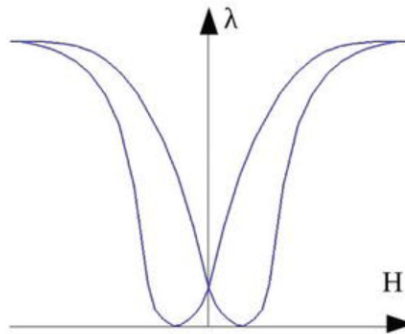


Figure 1.8: Typical magnetostriction curves in form of butterfly loop. ⁽¹¹⁾

As mentioned before, the magnetostriction can be characterized by a quadratic function, with the sign determined by the material rather than the direction of the applied magnetic field. Furthermore, the deformation is affected not only by the magnetic field, but also by other parameters such as the temperature. As the temperature increases, elongation reduces due to decreased magnetization. The magnetostriction curves are additionally influenced by the direction of the applied magnetic field, sample shape, chemical purity, and thermomagnetic history. The magnetostrictive effect is based on the rotation of the magnetization in the presence of an external magnetic field, which can result in novel magnetic domain configurations and either elongation or shrinkage of the magnetostrictive material. When a material is subjected to mechanical stresses or encounters an external magnetic field, the equilibrium of deformations attempts to minimize the total energy. When applied to crystalline magnets, uniaxial mechanical stress provides a magnetostrictive component to magnetic anisotropy; however, for polycrystalline materials, saturation magnetostriction represents an average.

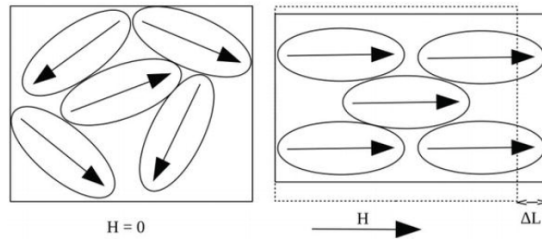


Figure 1.9: Schematic drawing depicting the magnetostriction caused by rotation of magnetization.⁽¹¹⁾

Magnetostrictive materials find valuable applications in the design of actuators and sensors. Utilizing both their magnetic and mechanical capabilities, these materials are widely used in sonar systems, the creation of industrial and medical ultrasonography, and the active control of noise and vibration.

Numerous magnetostrictive materials have been identified and they are classified into four categories: ferrites, iron-rare-earth alloys, amorphous alloys and Nickel and metallic crystalline alloys. Polycrystalline Nickel is a semi-soft magnetic substance that was the first magnetostrictive material to be employed as a transducer. It is characterized by:

- saturation magnetostrictive coefficient λ_s of -35 ppm: this coefficient corresponds to the strength of magnetoelastic coupling, can be either positive or negative;
- magnetomechanical coupling coefficient k_{33} of 0.3: k_{33} is a dimensionless parameter which describe the energy conversion ability from magnetic into

elastic energy and inversely.

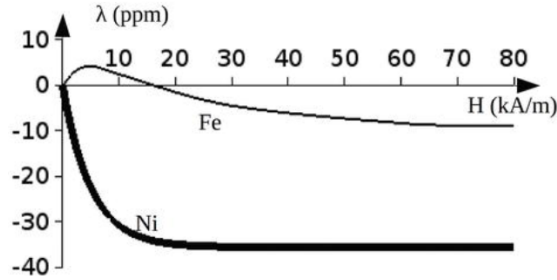


Figure 1.10: Magnetostriction curves characteristic of Ni (thick) and Fe(thin).⁽¹¹⁾

1.3 Single-phase ME materials: multiferroics

Multiferroics are a class of materials characterized by the simultaneous presence of, and a coupling between, the magnetic and ferroelectric orders. Although initially discovered and researched several decades ago, there has been increasing attention in this category of materials in recent times, driven by the ongoing quest for innovative multifunctional materials that can be used in the next generation of electronic devices. In these devices, magnetic spin is manipulated by electric fields, and viceversa the magnetic fields can be directly converted to electromotive forces.⁽¹²⁾ Such functionalities can have potential applications in spintronic devices, where the charge and spin degrees of freedom are employed to carry information. Other applications are for solid-state transformers, highly sensitive magnetic field sensors, and electromagneto-optic actuators. Within this category of materials, magnetism and ferroelectricity manifest independently. Magnetic order can occur through a variety of microscopic mechanisms, including as direct exchange (interaction of electrons on neighboring magnetic atoms, without intermediary), double exchange (the magnetic ions have mixed valence, so it can exist more than one oxidation state), indirect or superexchange interactions (indirect interaction between non-neighboring magnetic ions mediated by a non-magnetic ion), and it arises from electron spins and their interactions within the solid. Instead, electric order is more complex, with different mechanisms giving rise to ferroelectricity. These mechanisms consists in :

- off-center shifts of a cation relative to the surrounding anions, as observed in perovskites;
- lone-pair ferroelectricity, attributable to dangling bonds as seen in $BiFeO_3$;
- the ordering of charges as exemplified by Fe_3O_4 ;

- geometric effects, wherein distortion in the anion cage results in a closer lattice packing, thereby generating an electric dipole with respect to the central cation, as in $YMnO_3$.

The theoretical framework for understanding magnetoelectrics and multiferroics involves utilizing a series expansion of the free energy, taking into account the influences of magnetic and electric fields. The free energy density:⁽³⁾

$$dF = -SdT - P \cdot dE_0 - M \cdot dB_0 \quad (1.10)$$

written in S.I. units, where S is the entropy, T the temperature, P and M the electric and magnetic moments respectively. Lastly, E_0 and $B_0 = \mu_0 H_0$, are the external electric and magnetic fields respectively, where $\mu_0 = 4\pi \cdot 10^{-7} \text{VsA}^{-1}\text{m}^{-1}$ is the free space permeability. For a single phase multiferroic at constant temperature and up to quadratic order in the electric and magnetic field, the free energy is given by:

$$\begin{aligned} -F(E_0, B_0) = & P_S \cdot E_0 + M_S \cdot B_0 + \frac{\epsilon_0}{2} \sum_{ij} \chi_{ij}^e E_{0i} E_{0j} + \\ & + \frac{1}{2\mu_0} \sum_{ij} \chi_{ij}^m B_{0i} B_{0j} + \frac{1}{\mu_0} \sum_{ij} \alpha_{ij} E_{0i} B_{0j} + \dots \end{aligned} \quad (1.11)$$

where P_s and M_s are the electric and magnetic spontaneous polarization; χ^e and χ^m the electrical and magnetic susceptibility; ϵ_0 is the free space permittivity and α is the linear magnetoelectric coupling tensor, that appears to be very weak for single ME phase material. For what regards the multiferroics the total free energy of the system consists of the contribution of the electric and magnetic parts of the free energy that correspond to the magnetic and ferroelectric orders, while the magnetoelectric coupling term, that is not necessarily linear, describes the effective interaction between the order parameters of each phase

$$P_i = -\left(\frac{\partial F}{\partial E_{0i}}\right)_{B_0} = P_{si} + \epsilon_0 \sum_j \chi_{ij}^e E_{0j} + \frac{1}{\mu_0} \sum_j \alpha_{ij} B_{0j} + \dots \quad (1.12)$$

$$M_i = -\left(\frac{\partial F}{\partial B_{0i}}\right)_{E_0} = M_{si} + \frac{1}{\mu_0} \sum_j \chi_{ij}^m B_{0j} + \frac{1}{\mu_0} \sum_j \alpha_{ij} E_{0j} + \dots \quad (1.13)$$

showing that the effect of the magnetoelectric coupling is of inducing a new cross polarization component, in addition to the spontaneous and induced terms. For the linear magnetoelectric effect, it follows that :

$$\alpha_{ij} = \left(\frac{\partial P_i}{\partial B_{0j}}\right)_{E_0=B_0=0} = \mu_0 \left(\frac{\partial M_i}{\partial E_{0j}}\right)_{B_0=E_0=0} \quad (1.14)$$

For the isotropic material, the expression cited above becomes

$$\alpha^2 = \varepsilon_0 \mu_0 \chi^e \chi^m \quad (1.15)$$

and it is possible to demonstrate that for the single phase systems the expression for α_{ij} is:

$$\alpha_{ij} \leq \left(\varepsilon_0 \mu_0 \chi_{ii}^m \chi_{jj}^e \right)^{1/2} \quad (1.16)$$

and this set a physical limit to the size of the linear magnetoelectric effect. Example of these single phase intrinsic multiferroic compounds are:

- Perovskites $BiFeO_3$ is one of the most studied multiferroic materials, it is characterized by a large ferroelectric and magnetic ordering temperatures $T_N^e = 643$ K, $T_C^m = 1123$ K;
- the hexagonal manganites $RMnO_3$ (where R is a rare earth) are examples of improper ferroelectrics, with ferroelectricity being a byproduct of complex structural distortion.
- Fe_3O_4 (inverse spinel structure), it is a ferrimagnetic conductor with a Curie temperature $T_C^m = 850$ K, if the temperature decrease this material exhibits a structural transition from the cubic inverse spinel to an orthorombic structure at $T_N^e = 120$ K.

While the quest for novel intrinsic multiferroic materials continues, the small magnetoelectric coupling coefficients found in these material, and the fact that only a limited number of multiferroic are able to work at room temperature, have encouraged the development of heterogeneous material systems characterized by an artificial coupling between the order parameters of the ferroelectric and ferromagnetic components.

1.4 Conclusion

In conclusion, it can be stated that composite structures offer a highly effective technique to design new ME materials due to the favorable qualities of individual components magnetostrictive and piezoelectric. The development of strain-mediated composites made by single-phase compounds with large magnetic and piezoelectric responses was one of the earliest approaches to

magnetolectric coupling of materials. Within these composites, magnetolectric coupling arises from the mechanical strain that can induce deformation in the crystal structure of the magnetic phase via the converse piezoelectric effect or in the ferroelectric phase through magnetostriction. Consequently, when an electric field is applied to stimulate the composites, the converse piezoelectric effect leads to the generation of stress in the magnetic phase. The size of this effect depends on the relative amount of the ferroelectric polarization, the presence and absence of ferroelectric domain walls and conductivity in the composites (that can limit the strength of the applied magnetic field). The elastic coupling can also be subject to a reduction for the residual strains, grain boundaries and dislocation between the two phases.

In the direct magnetolectric coupling the presence of a stress field on the ferromagnetic phase induces changes in the magnetic anisotropy via magnetoelastic interactions that leads to modifications in the magnetic configuration. In this way there are some complications arising from the crystal orientation of the magnetic grains, that result in a non uniform change in the overall magnetic anisotropy, the presence of magnetic domain walls, pinning sites, residual strains and reduced magnetization. In the opposite process, the inverse magnetolectric effect, the magnetic field excites the composite modifying the magnetization alignment, which in turn causes a stress on the ferroelectric via magnetostriction and generate charges via piezoelectric effect.

This master thesis will focus on the understanding and experimental demonstration of this inverse version of the magnetolectric effect, focusion on one particular example of magnetostrictive-piezoelectric composites: Ni/PVDF-TrFe.

Chapter 2

Fabrication process and material characterization

As discussed in the previous chapter, a strong ME coupling can be expected in multilayer composite structures made of magnetostrictive/piezoelectric materials. The stack under investigation is consisted by PVDF-TrFe as piezoelectric layer and Ni as magnetostrictive layer.

2.1 Nickel

Nickel has been deposited on a substrate of Si/SiO_2 through two different techniques: Sputtering and thermal evaporation.

- **Sputtering deposition** is a quite diffused technique for depositing thin films. It is characterized by ion bombardment of a bulk material (referred to as the target).⁽¹⁴⁾

These ions are created from a gas (normally inert, e.g. Ar) in the deposition chamber. The bombardment leads to the target material's evaporation via a purely physical process based on kinetic energy transfer from the ions to the target atoms. Two different ways can be used to accelerate the ions: Direct current (DC) for conductive targets and radio frequency (RF) for nonconductive targets. A continuous electric field is used in DC sputter process to ionize and accelerate an inert sputtering gas toward the target. Depending on the applied gas pressure, these sputtered atoms will either move in a straight line in direction of the substrate (ballistic transport) or in a randomly way and deposit on all open surfaces (thermal

transport). The DC sputter process works very well for metal targets, such as Nickel.⁽¹⁵⁾

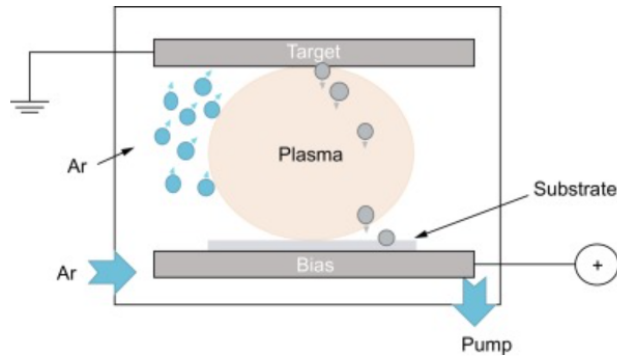


Figure 2.1: Schematic representation showing the standard sputtering technique.⁽¹⁶⁾

- **Thermal evaporation deposition** Another approach for depositing a thin layer is thermal evaporation. The source material evaporates in a vacuum chamber as a result of the high temperature heating. This temperature allows vapor particles to travel and condense into solids as they approach a substrate.⁽¹⁷⁾

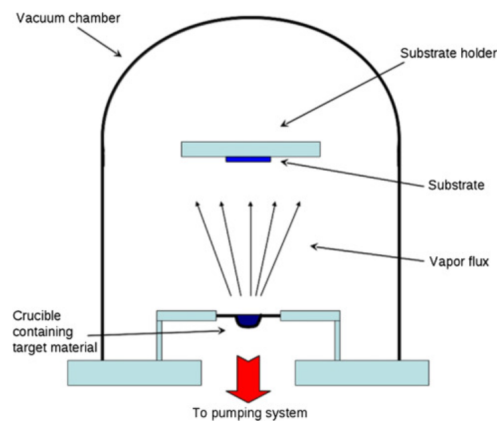


Figure 2.2: Schematic representation showing the thermal evaporation technique.⁽¹⁷⁾

2.1.1 Vibrating-sample magnetometry (VSM) analysis

The behavior of Ni deposited utilizing the two different procedures was investigated using vibrating-sample magnetometry (VSM). VSM is a scientific instrument used to measure magnetic properties. As shown in figure 2.3.a in this tool a magnetic sample is mounted on a sample holder and inserted between the horizontally oriented electromagnet poles. Depending on the type of measurements to be performed, the sample holder used for this tool can be of various types, with the option of selecting one for both In-Plane (IP) and Out-Of-Plane (OOP) measurements, or one for In-Plane (IP) measurements only, like shown in figure 2.3.b

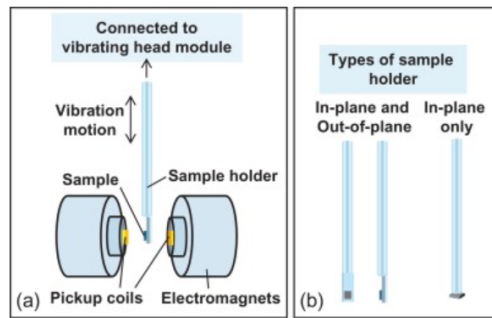


Figure 2.3: Schematic picture of (a) part of the VSM setup and (b) types of holder used in VSM.⁽¹⁸⁾

The sample needs to be placed in the right position, known as the "saddle point", which is determined by the calibration of the measurements. During the measurements the sample is subjected to a vertically constant vibration at a given frequency ω . The variation of the magnetic flux, which is proportional to the magnetic moment of the sample, induces an AC voltage induction, which can be monitored by a series of pickup coils located near the electromagnetic poles. The changing magnetic flux is revealed when the applied fields, coil location, or sample position are modified. The voltage induced is then supplied into a lock-in amplifier to determine the magnetic moment of the sample. Thanks to the use of VSM the magnetic properties of different stacks were analyzed:

- $Si/SiO_2 + 300$ nm Ni sputtered+ 20 nm of Tantalum
- $Si/SiO_2 + 300$ nm Ni sputtered+ 20 nm of Gold
- $Si/SiO_2 + 65$ nm Ni sputtered+ 100 nm of Gold
- $Si/SiO_2 + 300$ nm Ni evaporated+ 100 nm of Gold

Tantalum and Gold have been used in these stacks as a capping layer to prevent the oxidation of Nickel. Raw data obtained from the VSM show the values and graph of Magnetization (emu) vs Magnetic field (Oe). By dividing the magnetization values in emu for the volume of the magnetic layer it is possible to obtain the values of Magnetization (kA/m) vs Magnetic field (Oe), as shown in figure 2.4.

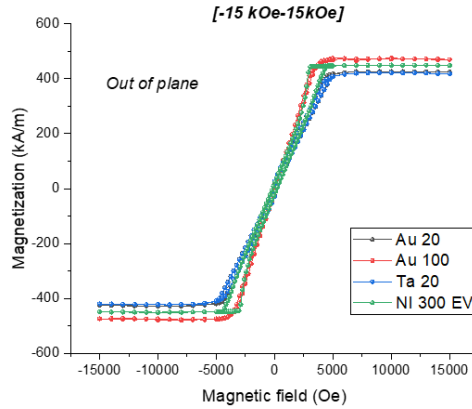


Figure 2.4: Hysteresis loop OUT OF PLANE Magnetization-Applied field for four different samples.

It is possible to see that the differences between the sample sputtered and the one evaporated are not relevant. In the same way, the use of different capping layers in the sputtered samples (Au 20 nm, Au 100 nm, Ta 20 nm), doesn't affect the magnetic properties of the Ni layer, demonstrating that in all the cases it is successfully protected by oxidation. It is also evident that the value at which the material reaches saturation are quite near, eventual small variations in this saturation value might be related to how the sample is positioned into the VSM; because it is manually inserted, there may be small differences in the saddle of the samples.

2.2 Nickel foil

Ni foils appears to be a very interesting material candidate to demonstrate the ME effect. PVDF layer is deposited on top of the Ni foil, and since Ni is a magnetostrictive material, this combination exhibits a significantly improved response to the deformation compared to the device fabricated with Ni dots on top of the PVDF-TrFe layer. This higher response may be attributable to the

absence of clamping effects on the PVDF layer when positioned on top of the Ni foil, since the full substrate is deforming by applying the external magnetic field. A sample of Ni foil was measured by VSM and the hysteresis loops for both magnetization Out Of Plane (OOP) and In Plane(IP) are shown in the figure 2.5.

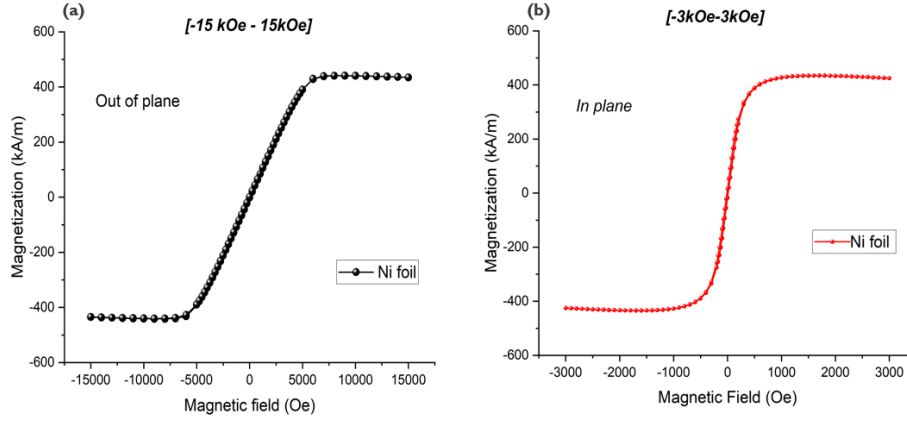


Figure 2.5: Hysteresis loop OUT OF PLANE Magnetization-Applied field (a) and IN PLANE Magnetization-Applied field (b) for Ni foil.

From the two different loops it is possible to extract the different values of remanence polarization, coercivity and saturation magnetization, shown in table 2.1.

At zero field, magnetic domains with completely random magnetization are

Table 2.1: Value of Hysteresis loop

OOP Magnetization		
Parameter	Negative	Positive
Remanance magnetization [kA/m]	-1.3977	1.3926
Coercivity [Oe]	-11.5015	11.9852
Saturation magnetization [kA/m]	-424.9058	434.49718
IP Magnetization		
Parameter	Negative	Positive
Remanance magnetization [kA/m]	-17.479	16.813
Coercivity [Oe]	-11.502	11.985
Saturation magnetization [kA/m]	-424.906	425.196

formed in the sample, and a magnetic field can be applied in order to align

them. As indicated in the table 2.1, the coercive field value is really small, this demonstrates that Ni is a soft material and is easy to magnetize it. Despite that, the saturation field value appears to be higher than the coercive field. The reason can be that fully align certain magnetic domain is pretty challenging. For example, at the edge or in defects, some magnetic domains are created and only a presence of a substantial magnetic force can alter their orientation. Moreover, the remanence, especially for the OOP magnetization, results to be really low. This suggests that in the absence of a magnetic field, the sample exhibits domain breakup, resulting in a near-zero net magnetization, with the domains effectively canceling each other out. In conclusion, it can be affirmed that this behavior of the Ni foil is attributable to the fact that the analysis pertains to a bulk material.

2.3 PVDF-TrFe

As previously discussed in the preceding chapter, in the examination of the Inverse Magnetoelectric effect within composite materials, the piezoelectric material of choice is PVDF-TrFe. The fabrication of this polymer consists in blending the powder of PVDF-TrFe with different possible solvents. For this particular thesis work, the powder used is Piezotech FC30 (30 % of TrFe) and the chosen solvent is MEK. This solution contains 55mg of PVDF-TrFe powder per 1 ml of MEK, which is mixed for two days until the PVDF powder is completely dissolved. The fabrication process continues with the spinning of the solution of PVDF-TrFe+MEK on the substrate $Si - SiO_2(400nm)/Ta(10nm)/Pt(100nm)$ or directly on the Ni foil, to obtain the device stack represented in figure 2.6.

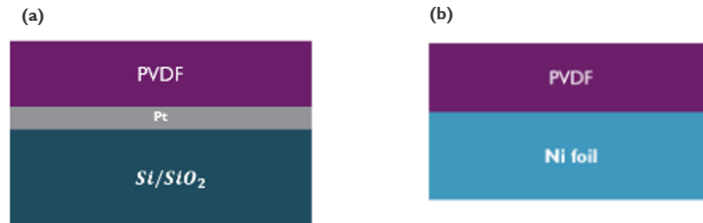


Figure 2.6: Schematic image of the two stacks: PVDF on Si/SiO_2 and Pt (a), PVDF on Ni foil (b).

Before the spinning of the solution of PVDF, the sample was cleaned first in Acetone at 50° , then in Isopropanol (IPA) at 75° and finally dried with a N_2

gun. The sample now is ready for the spin coating process, which consists of the following steps:

1. the sample was placed on a holder where the vacuum was applied;
2. the solution of PVDF was distributed over the entire sample through the use of a syringe;
3. a rotational velocity was applied in order to spread the solution over the substrate: in this case 4000 rpm for 30 seconds;
4. after the spinning the sample was transferred on a hot plate heated at 70° C for 1 minutes.



Figure 2.7: Schematic representation of the preparation of β -PVDF by spin coating. With the help of a syringe the PVDF solution is deposited on the substrate located on the rotary disk of the spin coater; proceed the deposition step at rotational velocity of 4000 rpm for 30 s; place the film onto a hot plate at 70 °C; and the PVDF film is ready.⁽¹⁹⁾

The fabrication process proceeds with the next two steps:

- 1)**Hard Baking:** Sample was baked in a Vacuum Oven for 4 hours and half at 70° C, followed by overnight cooling;
- 2)**Curing:** Sample was baked in a High Performance Oven for 1 hour at 140° C in N_2 atmosphere and successive cooling for 3 hours.

The next step of the fabrication for the two devices schematically represented in figure 2.6 is

- For a PVDF-TrFe spinned on $Si/SiO_2/Ta/Pt$ deposition of Nickel(Ni) and Gold (Au) on top of the PVDF-TrFE layer through the two different deposition techniques:
 - (1) Thermal evaporation of 300 nm of Ni and 100 nm of Au;
 - (2) Sputtering of 300 nm of Ni at low energy (150 W) and 100 nm of Au at higher energy (300 W)
- For PVDF-TrFe spinned on Ni foils deposition of 200 nm of Gold on top of the PVDF-TrFe layer through Thermal Evaporation.

Both depositions were done following the pattern of a shadowed mask. Thanks to this mask it was possible to fabricate the dots on top of the substrates with a variable dimensions: $60\ \mu\text{m}$, $90\ \mu\text{m}$, $120\ \mu\text{m}$, $150\ \mu\text{m}$, $200\ \mu\text{m}$, $300\ \mu\text{m}$, $400\ \mu\text{m}$ and $500\ \mu\text{m}$. The schematic pictures of the completed devices are shown in the following figure 2.8.

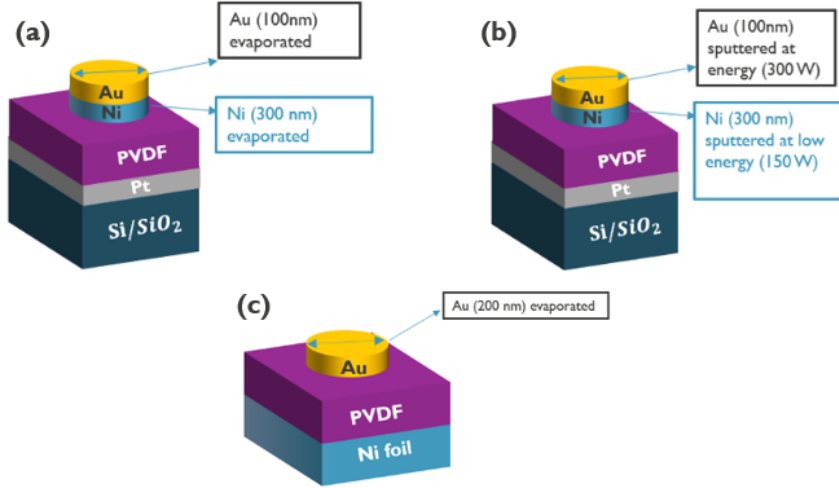


Figure 2.8: Schematic pictures of the final device: $Si/SiO_2/Ta/Pt/PVDF-TrFe$ and on top dots of Ni and Au evaporated (a), $Si/SiO_2/Ta/Pt/PVDF-TrFe$ and on top dots of Ni and Au sputtered (b), Ni foil+PVDF-TrFe on top dots of Au evaporated (c).

2.3.1 Polarization-Voltage loops

As fabricated PVDF-TrFe is in α phase and require to be polarized to switch in β phase. The polarization can be done by applying 80 V peak-to-peak triangular waves at 50 Hz for 200 pulses. Before the procedure of the poling is necessary to expose the bottom electrode of the samples. In the case of PVDF on $Si/SiO_2/Ta/Pt$ this procedure consists in the removal of the PVDF layer only in small corner of the sample. This can be done just using Acetone, since PVDF is effectively removed by Acetone; the sample is then cleaned using Isopropanol (IPA). In the case of PVDF on Ni foil, it is first necessary to glue the Ni foil on top of a substrate of gold using a silver paste, due to the fact that Ni foils are not so flat and require to be glued to flatter substrate to allow the measurement. These Ni foils are glued on a Si/SiO_2 substrate, on top of which a layer of Ti(10 nm)/Au(100 nm) was sputtered. This Au layer

has been used as the bottom electrode for the measurements reported in this thesis. The devices are analyzed using a probe station, the sample is placed on a chuck where vacuum is applied, one probe is connected to the previously exposed bottom electrode or to the gold substrate, and a second probe to the top electrode, the varying size dots on the device's top. These two probes are connected to the tool Keithley 4200, using before for the poling, as explained before and then for the P-V measurements. The results are shown in figure 2.9.

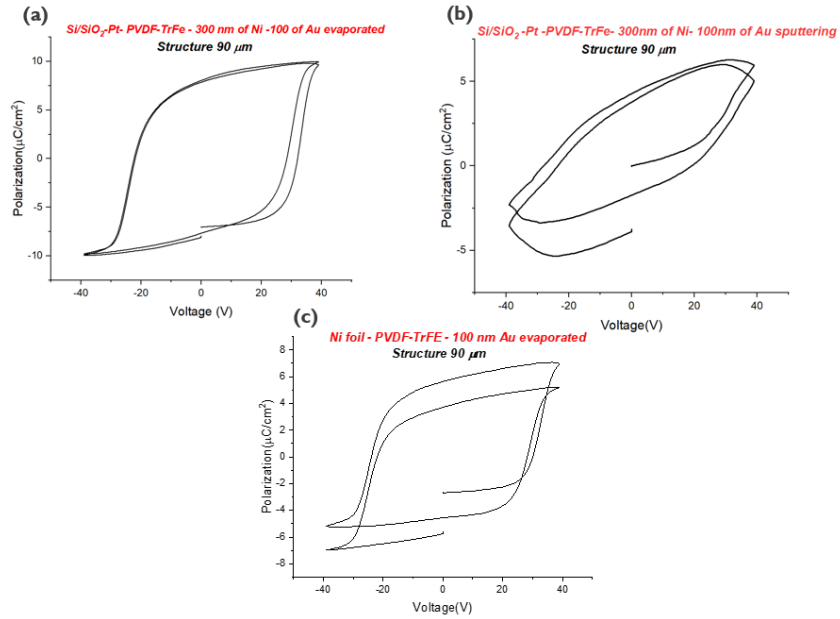


Figure 2.9: Polarization-Voltage (P-V) loop of the three different devices: Ni/Au evaporated (a), Ni/Au sputtered (b), Au evaporated (for PVDF-TrFe on Ni foil) (c).

The results show that when Ni and Au are sputtered on top of the substrate the P-V loop is extremely leaky. The cause can be that the atoms of the deposited material are implanted in the PVDF itself, since the energy at which they arrive on the surface is substantially higher than that of thermal evaporation. While, when Ni and Au are evaporated onto the substrate, they exhibit a clear P-V loop. The values for remanence, saturation, and coercive field for these two samples are listed in the table 2.2.

Table 2.2: Values of P-V loop

<i>Si/SiO₂-Pt-PVDF-TrFe-300 nm of Ni- 100 nm of Au evaporated</i>		
Parameter	Negative	Positive
Remanance magnetization [kA/m]	-8.0164	8.0577
Coercivity [Oe]	-21.9993	28.3419
Saturation magnetization [kA/m]	-9.96	9.96
Ni foil PVDF-TrFe- 100 nm Au evaporated		
Parameter	Negative	Positive
Remanance magnetization [kA/m]	-4.7973	4.6076
Coercivity [Oe]	-23.0586	26.9310
Saturation magnetization [kA/m]	-6.0869	6.0869

2.3.2 LCR meter measurements

LCR meter are largely used tool for the measurement of Impedance (L), Capacitance(C) and Resistance(R). This meter can also measure secondary parameters such as the dissipation factor (D) and the quality factor (Q). The dissipation factor D is the ratio of the real (resistance) to the imaginary (reactance) part of impedance; a low D corresponds to an early pure capacitor. The quality factor Q is the reciprocal of D value; a high Q corresponds to a more reactively pure components. Other parameters that can be measured with this kind of equipment to define an electrical component or material are: Conductance (G), Susceptance (B), phase angle and Equivalent Series Resistance (ESR). Various commercial LCR devices are available on the market, the Agilent E4989A/AL Precision LCR Meter is used for the following measurements, since it can apply a voltage bias up to 40V. The instrument displays a table or plot of measured results versus a test variable such as frequency, voltage or current. The user can define the sweep function's bottom and upper boundaries in Hz ,Volts or Amps, as well as the step or number of increments.⁽²⁰⁾

The following results show the measurement of Capacitance as a function of the DC bias Voltage, ranging from -35 V to 35 V in 1 V increments. When conducting a small signal capacitance-voltage sweep, a hysteresis loop, similar to a 'butterfly' loop, can be seen. These measurements are especially useful since they are correlated to the P-V loops showed before and they provide estimates of the saturation and coercive fields. The coercive voltage is represented as the point on the butterfly loop where the capacitance peaks. Furthermore, when the applied voltage is sufficiently high to saturate the film, the butterfly loop seems to 'pinch' off at the peak voltage. ⁽²¹⁾

The measurement are conducted for different dimensions of Ni dot evaporated on the top of the substrate: 60 μm , 90 μm , 120 μm , 150 μm , 200 μm , 300 μm , 400 μm and 500 μm ; and different frequencies: 1 kHz, 10 kHz, 100 kHz, 1 MHz.

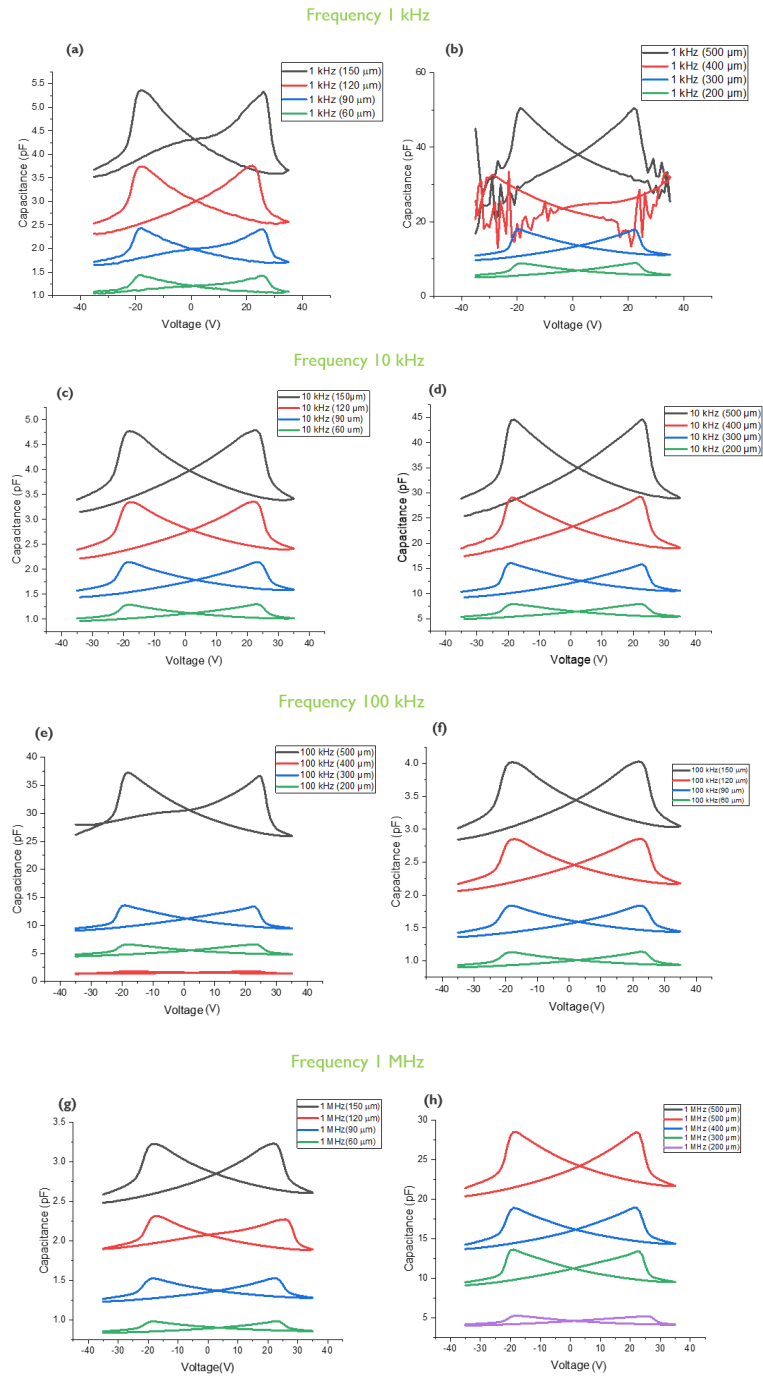


Figure 2.10: CV loops- Frequency 1 kHz(a,b), Frequency 10 kHz (c,d), Frequency 100 kHz (e,f), Frequency 1 MHz (g,h) for different structures: 60 μm , 90 μm , 120 μm , 150 μm [left] 200 μm , 300 μm , 400 μm and 500 μm [right].

The graphs above show that the Capacitance is directly proportional to the size of dots on top of the sample, as indicated by the formula $C = \epsilon_0 \epsilon_R \frac{A}{d}$, where A is the area of the Nickel dot, d is the thickness (500 nm), ϵ_0 and ϵ_R , the permittivity in the vacuum and the relative permittivity, respectively. Furthermore, the representation of how capacitance changes with frequency is shown in the figure 2.11. It is clear that as the frequency increases, the capacitance decreases. This behavior is due to the dielectric relaxation.

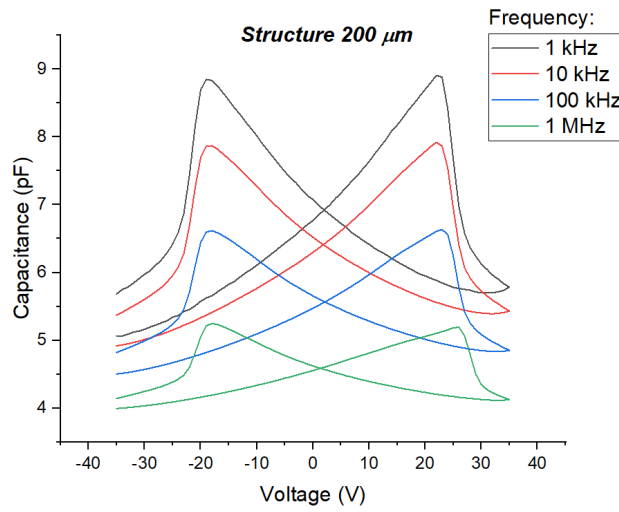


Figure 2.11: CV loops of the structure 200 μm at different frequencies: 1 kHz, 10 kHz, 100 kHz, 1 MHz.

The analysis continues with the calculation of the dielectric constant ϵ_R . From the value of Capacitance it is possible to obtain the value of ϵ_R through the inverse formula: $\epsilon_R = \frac{Cd}{\epsilon_0 A}$

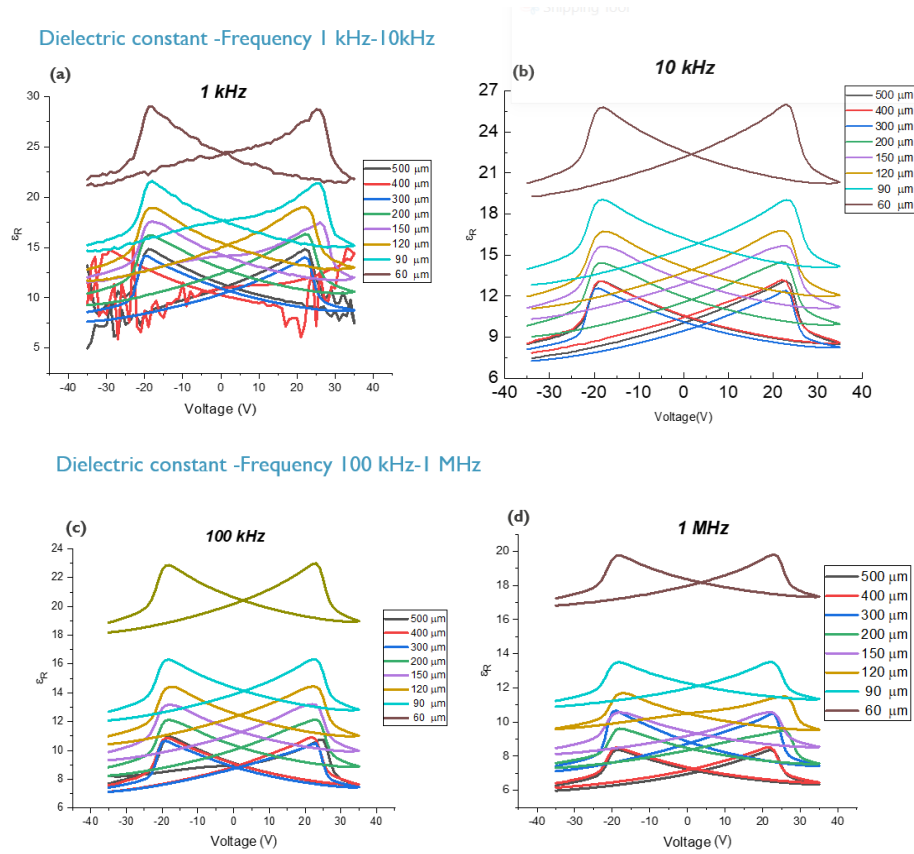


Figure 2.12: Dielectric constant (ϵ_R)- Frequency 1 kHz(a), Frequency 10 kHz(b), Frequency 100 kHz(c), Frequency 1 MHz (d) for different structures: 60 μm , 90 μm , 120 μm , 150 μm , 200 μm , 300 μm , 400 μm and 500 μm .

The expected results were that the dielectric constant would be consistent for all dimensions. This discrepancy may arise from the presence of a parallel parasitic capacitance, likely caused by the connection of cables from the LCR to the probes attached to the device, that can be added to the Capacitance of the device itself. For the generation of devices fabricated with PVDF-TrFe on top of Ni foil, the measurements of Capacitance with LCR meter result to be similar.

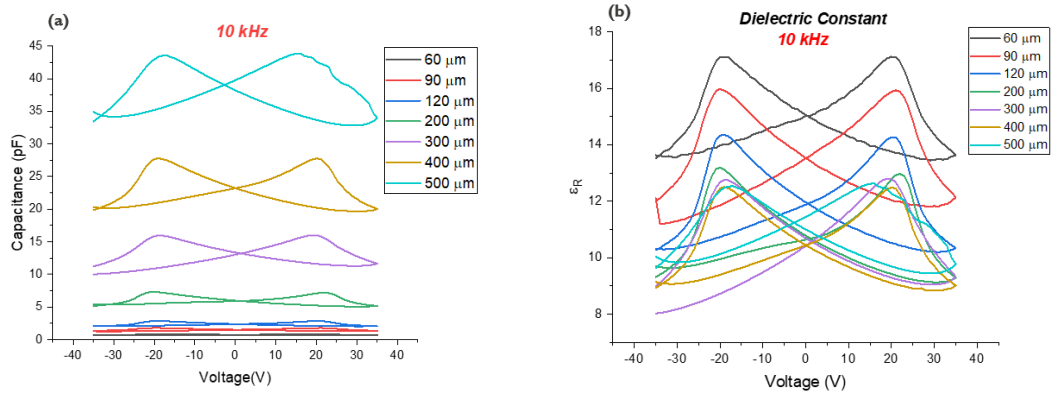


Figure 2.13: CV loops for device : Ni foil/PVDF-TrFe/Au evaporated- Frequency 10 kHz (a), Dielectric constant (ϵ_R)- Frequency 10 kHz (b) for different structures: 60 μm , 90 μm , 120 μm , 150 μm , 200 μm , 300 μm , 400 μm and 500 μm .

Chapter 3

Inverse ME effect measurements

The inverse magnetoelectric effect, as previously mentioned in the preceding sections, is a phenomenon in which the application of a magnetic field (H) causes a change of electric polarization (P). The focus of this chapter is to investigate the electric behavior of our device when it is exposed to a magnetic field.

3.0.1 Description of the setup and measurement technique

To analyze how the device behaves when subjected to a magnetic field, a specific setup shown in the figure 3.1.a was employed. In this setup, it is possible to simultaneously apply both Out Of Plane and In Plane magnetic fields, generated by two magnets with two magnetic poles per each, as shown in figure 3.1.b

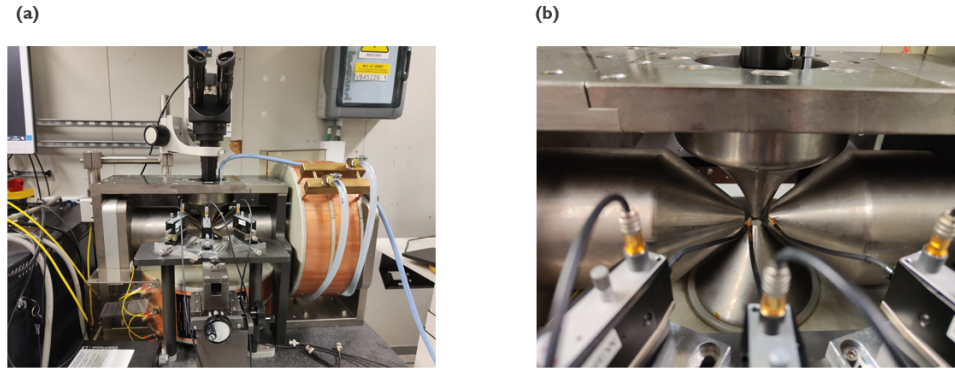


Figure 3.1: Picture of the setup used for inverse ME measurements (a), zoom on the magnets (b).

A sample with a maximum size of 1 cm*1 cm is placed on a holder and taped to it. Two probes are connected to the sample after the holder is positioned into the zone where magnetic fields are applied. One probe is connected to the common bottom electrode (the exposed Pt bottom electrode or the $Si/SiO_2/Au$ substrate as described in the previous chapter). The other is connected to the top electrode, the dots of varying sizes on PVDF-TrFe.

The applied magnetic fields for this device range in the case of Out Of Plane (OOP) from -1 Tesla to 0 and from 1 Tesla to 0, while the In Plane (IP) magnetic field remains constant at 500 Oe (0.05 T). The out-of-plane (OOP) field range was chosen in this way to fully encompass the hysteresis curve of Ni. The in-plane (IP) field, on the other hand, is set at either 0 or 500 Oe to fully magnetize the In-Plane Nickel. This approach allows for a theoretical comparison between the scenario where domains transition from completely random (Ni unmagnetized) to gradually achieving OOP magnetization, and the case where the transition occurs from in-plane (IP) domains to out-of-plane (OOP) domains (rotation of Ni magnetization from IP to OOP). Also for this type of measurements, each time PVDF-TrFe requires to be polarized to switch to β -phase and preserve its ferroelectricity by applying 80 V peak-to-peak triangular waves at 50 Hz for 200 pulses. The P-V loop is measured in relation to the OOP magnetic field. The device is poling with the Keithley 4200 instrument, which is connected to the setup's probes via appropriate connections.

3.1 Inverse ME effect measurements for the device: $Si - SiO_2/Ta/Pt$ - PVDF-TrFe- Ni and Au dots

The first generation of devices analyzed has $Si - SiO_2/Ta/Pt$ - PVDF-TrFe-Ni and Au dots evaporated on top. For each variable size dots on top of the substrate were conducted the measurements in this way:

1. First polarization of PVDF-TrFe (200 pulses) without the application of a magnetic field;
2. Application of OOP magnetic field switching from -1 Tesla to 0 and from 1 Tesla to 0, and last measurement applying again -1 Tesla, repeating the poling (200 pulses) each time;
3. Application of a constant IP magnetic field 500 Oe (0.05 T) and simultaneous application of OOP magnetic field switching from -1 Tesla to 0 and from 1 Tesla to 0, and last measurement applying again -1 Tesla, repeating the poling (200 pulses) each time.

It is possible to estimate the value of the expected polarization variation by taking into account the properties of the material of the device.

Polarization variation expected

From d_{33} coefficient:

- $d_{33}^{PVDF} = 33 \text{ pC/N}$; $\lambda_{Ni} = 60 \text{ ppm}$; $Y_{PVDF} = 2.17 \text{ GPa}$
- $T(\text{stress}) = \lambda_{Ni} * Y_{PVDF} = 13 * 10^4 \text{ Pa}$
- $P(\text{polarization}) = Q(\text{charges})/A = (d_{33}^{PVDF} * T * A)/A = d_{33}^{PVDF} * T = 429 * 10^4 \text{ pC/m}^2$
- $P = 4.29 * 10^{-4} \text{ } \mu\text{C/cm}^2$

From g_{33} coefficient:

- $g_{33}^{PVDF} = 287 * 10^{-3} \text{ Vm/N}$; $\lambda_{Ni} = 60 \text{ ppm}$; $Y_{PVDF} = 2.17 \text{ GPa}$
- $T(\text{stress}) = \lambda_{Ni} * Y_{PVDF} = 13 * 10^4 \text{ Pa}$
- $P(\text{polarization}) = Q(\text{charges})/A = (C(\text{capacitance}) * V(\text{voltage}))/A = (\epsilon * A * g_{33}^{PVDF} * T * d(\text{thickness}))/A * d = \epsilon * g_{33}^{PVDF} * T = 3.31 * 10^{-6} \text{ C/m}^2$
- $P = 3.32 * 10^{-4} \text{ } \mu\text{C/cm}^2$

The expected value is very low, so achieving this value will be very challenging.

In the figure 3.2 the representation of Polarization-Voltage P-V loops for a structure with dot diameter of $300 \mu\text{m}$.

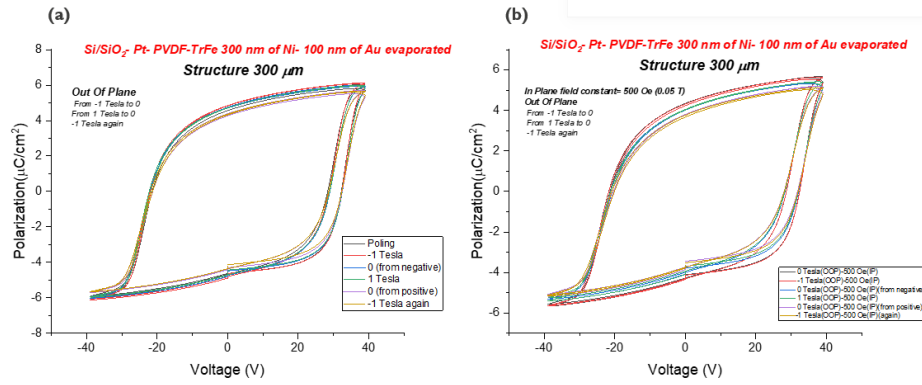


Figure 3.2: PV loops of the structure $300 \mu\text{m}$ applying: (a) OOP magnetic field from -1 Tesla to 0 and from 1 Tesla to 0 (b) IP magnetic field constant 500 Oe (0.05 T) and OOP magnetic field from -1 Tesla to 0 and from 1 Tesla to 0.

The expected results were that the loop measured at 1 Tesla and -1 Tesla would overlap, since the magnetostrictive effect in Ni is expected to be symmetric for rotations of 180° of the magnetization. However they appear displaced, with the area of the 1 Tesla loop reduced. This behavior can be further investigated by analyzing key loop parameters like remanence polarization, coercivity, and saturation with the magnetic field. In the figure 3.3(a,b) below, the variation of both positive and negative remanence polarization is shown as a function of the OOP magnetic field range from -1 Tesla to 0 and from 1 Tesla to 0 and as function of the number of measurements performed.

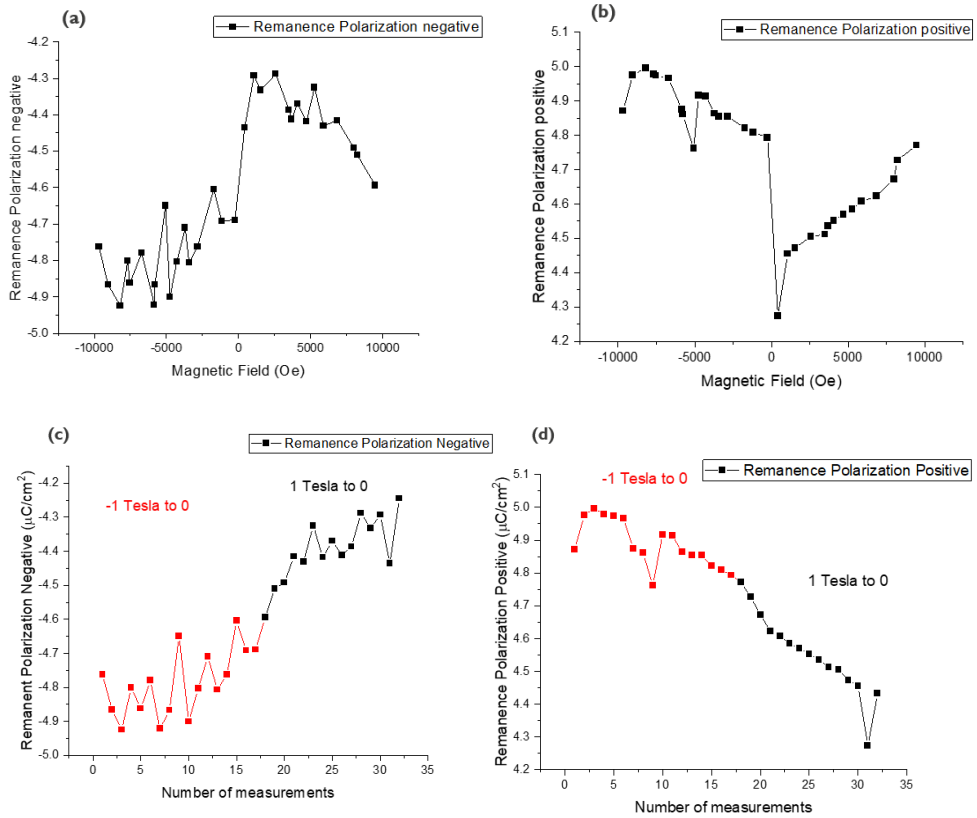


Figure 3.3: Representation of how remanence polarization varies applying a OOP magnetic field (from -1 Tesla to 0 and from 1 Tesla to 0) for a structure of $300 \mu\text{m}$: negative remanence (a) and positive remanence(b), Representation of how remanence polarization varies with the number of measurements for a structure of $300 \mu\text{m}$: negative remanence (c) and positive remanence(d).

It is possible to observe that in figures 3.3.a and 3.3.b the trend of the graph with the magnetic field is not so symmetrical. However, when evaluating the variation of remanence polarization over time, based on the number of measurements conducted, the graph appears much more linear. This trend is not due to the applied magnetic field, but rather to the fact that the material undergoes degradation. Infact, as shown in the graph of the negative remanence polarization in figure 3.3.c, the value increases with the number of measurements, while the positive remanence in figure 3.3.d tends to decrease. These findings strongly indicate that the material undergoes degradation during the measurement process. This degradation can depend on experimental parameters such as temperature, the type of electrodes, and

the frequency and amplitude of the applied wave. It has been observed that degradation becomes more pronounced with higher driving voltage and lower frequency. Moreover, given the semicrystalline nature of ferroelectric polymers, the degree of crystallinity can also influence degradation. Specifically, charges trapped in defects and crystalline regions may impede domain walls and reduce the polarization.⁽²²⁾

This degradation is also evident evaluating how varies the saturation and coercivity with the number of measurements, as shown in figures below.

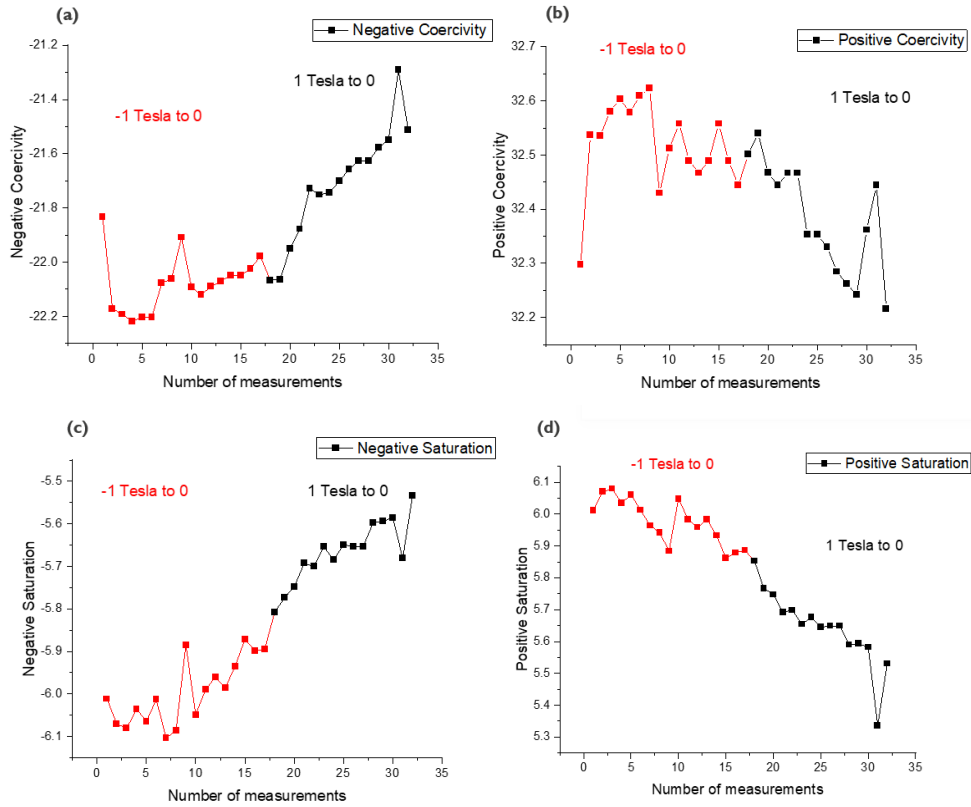


Figure 3.4: Representation of how coercive field and saturation varies with the application of magnetic field with the number of measurements for a structure of 300 μm : negative coercivity (a) and positive coercivity (b), negative saturation (c), positive saturation (d).

This degradation is expected to be enhanced by the poling step, since before each measurements 200 triangular waves with 80 V peak-to-peak of amplitude are applied. Therefore, to mitigate this degradation issue, one potential solution involves reducing the number of pulses in the poling step from 200 to 10. The proposed approach entails conducting an initial polarization with 200

pulses to switch the PVDF-TrFe in β phase and subsequently reducing the number of pulses to 10 for the next measurements. This 10 pulses between each measurements are needed to keep the PVDF in β phase for the whole measurements procedure. To test if this loops reduction has a reasonable effect on the degradation, 100 P-V loops measurements without applying any magnetic field have been performed with both the poling procedures. The result obtained measuring a device with $400 \mu\text{m}$ of diameter are shown in figure 3.5.

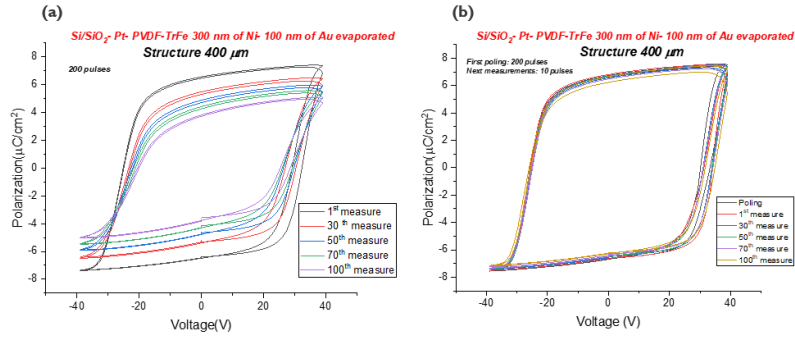


Figure 3.5: 100 Polarization-Voltage (P-V) loops for a structure of $400 \mu\text{m}$: (a) Initial Poling (200 pulses) + successive measurements (10 pulses); (b) Initial poling (200 pulses) + successive measurements (200 pulses).

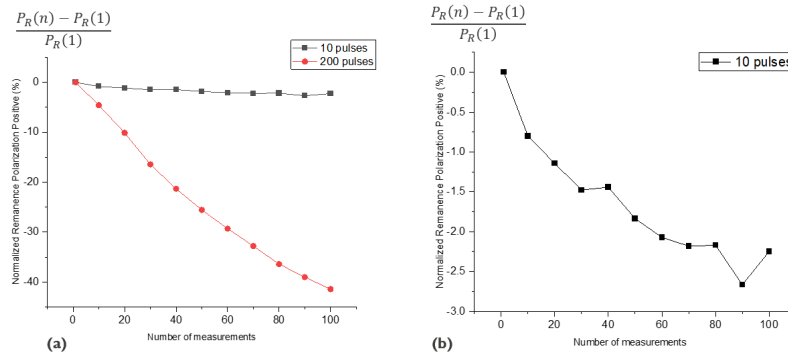


Figure 3.6: Representation of how normalized Remanence Polarization for a structure of $400 \mu\text{m}$ varies: (a) Comparison of 100 measurements conducted with 200 pulses or 10 pulses; (b) Zoom on the measurements with 10 pulses.

The almost coincident loops indicate that this technique is highly promising, as deterioration is reduced. Most crucially, despite the reduction of the number of loops, the material retains its ferroelectric characteristics. Moreover, the

figure 3.6 shows that after 100 measurements, the Remanence polarization for the measurement with 200 pulses varies by 40 %, while for the one with 10 pulses, it varies by 2.5 %. This is another demonstration that this technique is very promising.

3.2 Inverse ME effect measurements for the device: PVDF-TrFe on Ni foil

The second generation of analyzed devices consists of those Ni foil-PVDF-TrFe with Au evaporated on top. Measurements were conducted for various dot sizes on the substrate, using the same methods stated in the previous section for the first generation of devices. Furthermore, in this case, the solution to minimize material degradation by reducing the number of poling steps to 10 has been implemented. In figure 3.7, P-V loops for this device are depicted. The observed degradation appears to be minimal, as there is no significant shift in the measured loops over time.

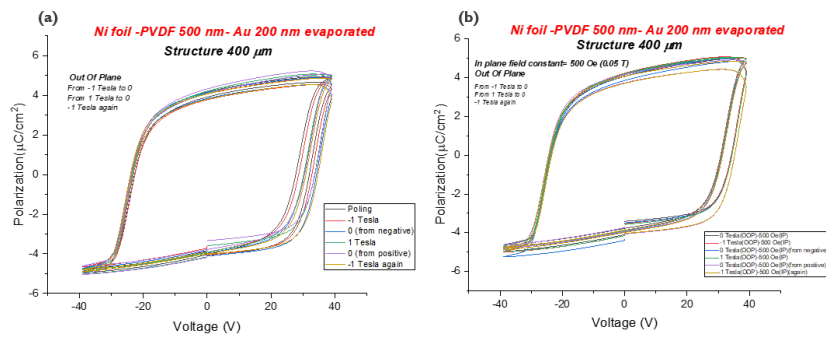


Figure 3.7: Polarization-Voltage (P-V) loop for a structure of 400 μm for a device fabricated with PVDF layer on top of Ni foil: OOP field (a), IP field constant OOP field variable (b).

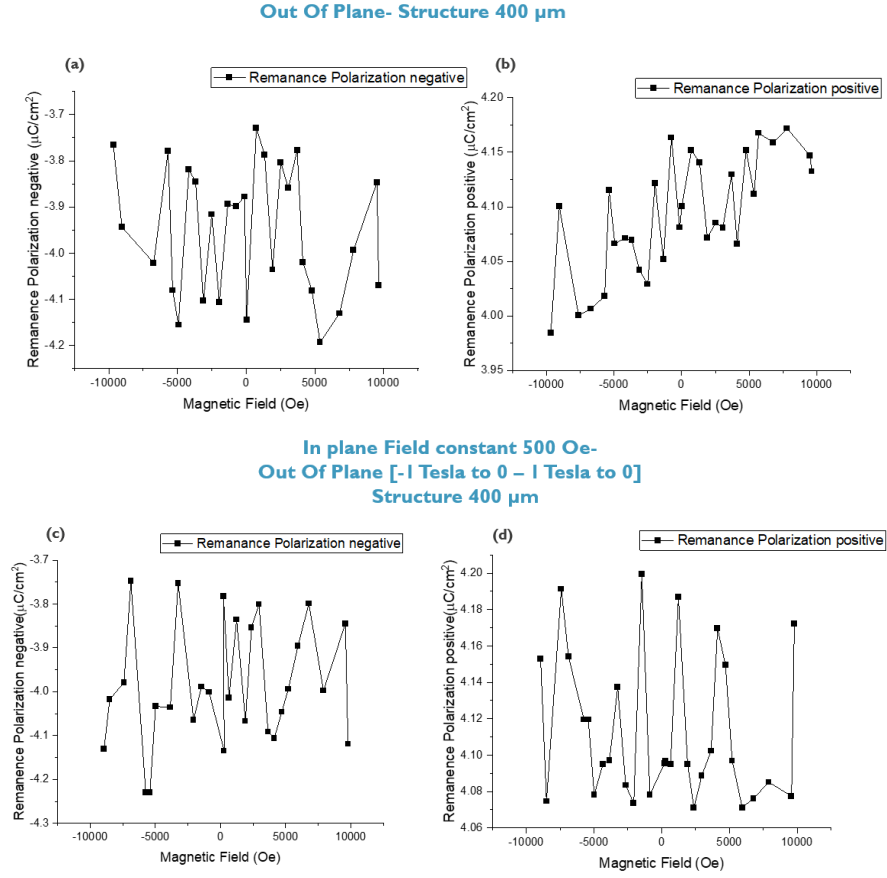


Figure 3.8: Representation of how positive and negative remanence polarization varies with the application of magnetic field OOP [-1 Tesla to 0 and 1 Tesla to 0](a,b) and IP CONSTANT [500 Oe]- OOP [-1 Tesla to 0 and 1 Tesla to 0] (c,d) for a structure of 400. μm

To analyze the data represented in the figure 3.8, the error was calculated using the standard deviation :

$$\sigma = \sqrt{\frac{\sum_{i=1}^N (x_i - \bar{x})^2}{N}} \quad (3.1)$$

where:

- σ is the standard deviation;
- N is the total number of observations;
- x_i are the individual observations;
- \bar{x} is the mean of the observations,

assuming that there is no variation in polarization due to the effects of degradation and the magnetic field. In this way, the error in the measurement is attributed solely to noise. The measurement error relative to the noise for positive remanence polarization is approximately $0.04 \mu\text{C}/\text{cm}^2$, while for negative remanence polarization, it is about $0.14 \mu\text{C}/\text{cm}^2$. This noise is much higher compared to the expected polarization variation ($\Delta P \approx 10^{-4}$), and for this reason it is not possible to observe a dependence of polarization with the magnetic field.

3.3 Outlook

To solve this noise issue, there are several potential solutions. One initial approach could involve the reduction of the noise. This noise may result from various factors, such as the possibility that the setup used may not be adequately isolated, or that the Ni foil, being a magnetic material, could undergo displacement due to the attraction of the surrounding magnetic field once inserted into the setup. In this specific setup, creating a vacuum condition is not feasible, and the device is fixed on the holder using adhesive tape. Therefore, a solution to prevent the sample from moving during measurements could be to use double-sided tape. If it is not possible to significantly reduce this noise, an alternative solution may be the charge measurements.

3.3.1 Charge measurements

The polarization value is not affected by the size of the measured dots on top of the substrate but solely depends on the material's properties, there is no method to increase the expected polarization change. On the other hand, the magnetoelectric generated charges depends on the size of the measured area. Consequently, with larger structures, it is possible to increase the quantity of generated charge to surpass the level of noise produced. This is demonstrated by the measurements in the figure 3.9.

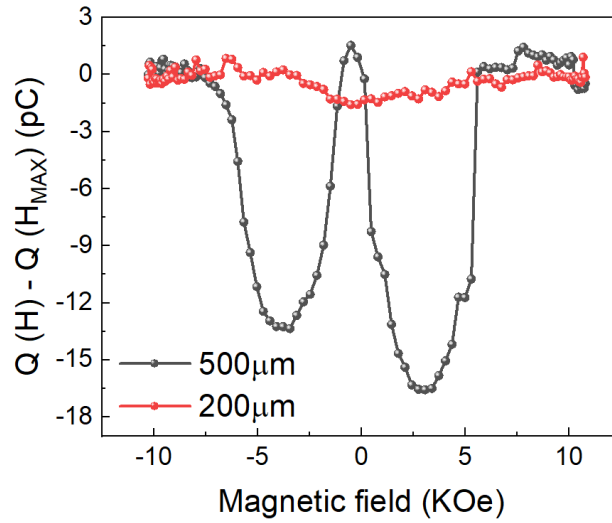


Figure 3.9: Representation of charge induced by ME effect for a structure of 200 μm and 500 μm .

Measurements were conducted by simultaneously applying an out-of-plane (OOP) magnetic field and a fixed in-plane (IP) magnetic field at 500 Oe. The measurement of charges induced by the magnetoelectric (ME) effect varies only in the region of change (where strain changes with the magnetic field), while it remains constant in the saturation region. The amount of charge generated for the structure at 200 is approximately 2 pC, while that generated for the measurement at 500 is about 500 pC.

Chapter 4

Conclusions

In this thesis work, the inverse magnetoelectric effect has been demonstrated for a multilayer composite consisting of a stack of piezoelectric (PVDF-TrFe) and magnetostrictive (Ni) layers. The fabrication process involved spinning a 500 nm thick PVDF-TrFe layer on either $Si-SiO_2(400nm)/Ta(10nm)/Pt(100nm)$ substrate or directly on a Ni foil substrate. Subsequently, Ni and Au were deposited on both devices according to the pattern provided by a round shadowed mask.

The PVDF-TrFe layer was subjected to 80 V peak-to-peak triangular waves at 50 Hz for 200 pulses, to allow its transition from the α -phase to the β -phase characterized by the highest dipolar moment. The ferroelectric and piezoelectric behavior of PVDF-TrFe was demonstrated by measuring its Polarization-Voltage (P-V) loop, which, in the case of the sputtered sample, was found to be very leaky due to atom implantation in the PVDF layer. Instead, when Ni and Au have evaporated above the PVDF-TrFe, the P-V loop shows the correct ferroelectric behavior.

Subsequent measurements in a magnetic field involved the simultaneous application of an In-Plane (IP) and Out-Of-Plane (OOP) magnetic field. The OOP magnetic field varied from -1 Tesla to 0 and from 1 Tesla to 0, while the IP field was fixed at 500 Oe (0.05 T). The PVDF layer was poled for every measurement under the previously mentioned conditions, and its P-V loop was measured as a function of the OOP magnetic field.

From the initial results, it emerged that the material undergoes degradation during the measurements. A promising solution was adopted, which involved reducing the number of pulses in the poling step to 10 for each measurement. By comparing the graph of the normalized remanence polarization variation, it was observed that this degradation was reduced from 40% for measurements

with 200 pulses to 2.5% for measurements with 10 pulses.

Subsequently, the variation of polarization with the magnetic field was evaluated. The measurement error relative to the noise was approximately 0.04 for positive remanence polarization and 0.14 for negative remanence polarization. This noise is much higher compared to the expected polarization variation ($\Delta P \approx 10^{-4}$), making it impossible to observe a dependence of polarization on the magnetic field.

To reduce this noise, one possible solution could be to use double-sided tape. An additional proposed approach would be to proceed with the measurement of charge. The magnetoelectric generated charges depend on the size of the measured area. Consequently, with larger structures, it is possible to increase the quantity of generated charge to surpass the level of noise produced.

Chapter 5

Bibliography

- 1) P. Curie, J. Physique 3e series, 3, 393 (1894).
- 2) L.D. Landau and E. Lifshitz, Electrodynamics of Continuous Media (Addison-Wesley: Translation of a Russian edition of 1958), (1960).
- 3) I.E. Dzyaloshinskii, Sov. Phys.—JETP, 37, 628 (1960).
- 4) M. Fiebig, J. Phys. D: Appl. Phys. 38, R123 (2005).
- 5) T. H. O'Dell, "The Electrodynamics of Magneto-Electric Media" (North-Holland, Amsterdam, 1970).
- 6) R. R. Birss, Symmetry and Magnetism (North-Holland, Amsterdam, 1964).
- 7) D.N.Astrov , "The Magnetoelectric effect in antiferromagnetic" ,(1960).
- 8) Fundamentals of Piezoelectricity.
- 9) Xiongjie Li¹, Yiping Wang¹, Tingrui He, Querui Hu, Ying Yang, "Preparation of PVDF flexible piezoelectric film with high β -phase content by matching solvent dipole moment and crystallization temperature" , (2019).
- 10) G. Gutiérrez-Sánchez¹, J. Hernando-García¹, Victor Ruiz-Diez¹, O.J. Dura, M.A. López de la Torre, J.L. Sánchez-Rojas, "Comparative assessment of PVDF and PVDF-TrFE piezoelectric polymers for flexible actuators applications" ,(2017).
- 11) Yannick Le Bras and Jean-Marc Greneche, "Magneto-Elastic Resonance: Principles, Modeling and Applications" ,(2017).
- 12) C A F Vaz , "Electric field control of magnetism in multiferroic heterostructures" , (2012).
- 13) David Boldrin, Andrei P. Mihai, Bin Zou, Jan Zemen, Ryan Thompson, Ecaterina Ware, Bogdan V. Neamtu, Luis Ghivelder, Bryan Esser, David W. McComb, Peter Petrov, and Lesley F. Cohen, "Giant Piezomagnetism in Mn₃NiN" ,(2018).
- 14) D. Depla, S. Mahieu, J.E. Greene, "Sputter Deposition Processes- Chapter 5" , (2019).
- 15) Vladimir Kolkovsky, Ronald Stübner Fraunhofer IPMS, "Point defects in

- stoichiometric and nonstoichiometric metal oxides for modern microelectronics", (2023).
- 16) Muhammad S. Zafar, Sana Zohaib, "Bioactive Surface Coatings for Enhancing Osseointegration of Dental Implants" (2019).
- 17) Almas Bashir, Tahir Iqbal Awan, Aqsa Tehseen, Muhammad Bilal Tahir, Mohsin Ijaz, "Interfaces and surfaces", (2020).
- 18) A.O. Adeyeye, G. Shimon, "Magnetism of Surfaces, Interfaces, and Nanoscale Materials", (2015).
- 19) Carlos M Costa, Daniela M Correia, João Nunes-Pereira, Juliana Oliveira¹, Pedro Martins¹, Renato Gonçalves, Vanessa F Cardoso, Senentxu Lanceros-Méndez, " Electroactive poly(vinylidene fluoride)-based structures for advanced applications", (2018).
- 20) Mitar Simić, "Realization of Digital LCR Meter", (2014).
- 21) Timothy James Reece, Ph.D., "Characterization of Metalferroelectric-Insulator-Semiconductor Structures Based on Ferroelectric Langmuir-Blodgett Polyvinylidene Fluoride Copolymer Films for Nondestructive Random Access Memory Applications", (2007).
- 22) Dong Zhao, Ilias Katsouras¹, Mengyuan Li, Kamal Asadi, Junto Tsurumi, Gunnar Glasser, Jun Takeya, Paul W. M. Blom¹ Dago M. de Leeuw, "Polarization fatigue of organic ferroelectric capacitors", (2014).